Author/s:
Freeman, AJ;Vervoort, SJ;Michie, J;Ramsbottom, KM;Silke, J;Kearney, CJ;Oliaro, J

Title:
HOIP limits anti-tumor immunity by protecting against combined TNF and IFN-gamma-induced apoptosis

Date:
2021-11-04

Citation:
Freeman, A. J., Vervoort, S. J., Michie, J., Ramsbottom, K. M., Silke, J., Kearney, C. J. & Oliaro, J. (2021). HOIP limits anti-tumor immunity by protecting against combined TNF and IFN-gamma-induced apoptosis. EMBO Reports, 22 (11), https://doi.org/10.15252/embr.202153391.

Persistent Link:
https://hdl.handle.net/11343/338025

HOIP limits anti-tumor immunity by protecting against combined TNF and IFN-gamma induced apoptosis

Andrew J Freeman[1,3], Stephin J Vervoort[2,3], Jessica Michie[1,3], Kelly M Ramsbottom[1], John Silke[4,5], Conor J Kearney[2,3,*], and Jane Oliaro[1,3,6,7,*]

[1]Cancer Immunology Program, Peter MacCallum Cancer Centre, Melbourne, Victoria 3000, Australia

[2]Translational Haematology Program, Peter MacCallum Cancer Centre, Melbourne, Victoria 3000, Australia

[3]Sir Peter MacCallum Department of Oncology, The University of Melbourne, Victoria 3010, Australia

[4]Inflammation Department, Walter and Eliza Hall Institute of Medical Research, Victoria 3010, Australia

[5]Department of Medical Biology, The University of Melbourne, Victoria 3010, Australia

[6]Department of Immunology and Pathology, Monash University, Victoria 3004, Australia

[7]Correspondence: jane.oliaro@petermac.org (J.O.)

*These authors contributed equally to this work

Running title: HOIP limits anti-tumor immunity

Keywords: CRISPR screen / HOIP / IFN-gamma / Immunotherapy / TNF

ABSTRACT

The success of cancer immunotherapy is limited to a subset of patients, highlighting the need to identify the processes by which tumors evade immunity. Using CRISPR/Cas9 screening, we reveal that melanoma cells lacking HOIP, the catalytic subunit of LUBAC, are highly susceptible to both NK and $CD8^+$ T cell-mediated killing. We demonstrate that HOIP-deficient tumor cells exhibit increased sensitivity to the combined effect of the inflammatory cytokines, TNF and IFN-γ, released by NK and $CD8^+$ T cells upon target recognition. Both genetic deletion and pharmacological inhibition of HOIP augments tumor cell sensitivity to combined TNF and IFN-γ. Together, we unveil a protective regulatory axis, involving HOIP, which limits a transcription-dependent form of cell death that engages both intrinsic and extrinsic apoptotic machinery upon exposure to TNF and IFN-γ. Our findings highlight HOIP inhibition as a potential strategy to harness and enhance the killing capacity of TNF and IFN-γ during immunotherapy.

INTRODUCTION

The treatment of several cancer types, particularly metastatic melanoma, has been transformed by immunotherapy. Current forms of immunotherapy include releasing the 'brake' on tumor-specific cytotoxic $CD8^+$ T lymphocyte activity through blockade of suppressive checkpoint receptor/ligand interactions (Ribas *et al*, 2016), as well as the adoptive transfer of chimeric antigen receptor T cells genetically engineered to recognize and kill target cells expressing a particular tumor antigen (Maude *et al*, 2015). Despite the efficacy of these therapies, only a subset of patients benefit due to both acquired and intrinsic resistance (Shi *et al*, 2020), highlighting the need for a better understanding of the proteins and pathways that mediate tumor immune evasion. Identification of these processes is essential for the development of novel therapeutics that may augment anti-tumor immune responses, and lead to more patients achieving durable responses to immunotherapy.

Although $CD8^+$ T cells are the primary target for currently approved immunotherapies, natural killer (NK) cells are increasingly being recognized as an additional and essential cell type involved in the anti-tumor immune response and exhibit promising potential as an additional immunotherapy target, primarily due to their capacity to potently kill major histocompatibility complex I (MHC-I) negative tumor cells (Souza-Fonseca-Guimaraes *et al*, 2019). $CD8^+$ T cells and NK cells can directly destroy malignantly transformed cells through the release of lytic proteins, including perforin and granzymes. Additionally, these cytotoxic lymphocytes also produce and secrete pro-inflammatory cytokines upon target recognition, including tumor necrosis factor (TNF) and interferon-gamma (IFN-γ), which elicit pleiotropic effects within the tumor microenvironment following binding to their respective cognate receptors.

We recently conducted a genome-wide *in vitro* clustered regularly interspaced short palindromic repeat (CRISPR)/CRISPR-associated protein 9 (Cas9) screen in B16-F10 mouse melanoma cells to

identify genes, that when deleted, confer sensitivity to killing by NK cells (Freeman *et al*, 2019). In addition to known tumor regulators of NK cell killing, this screen also identified genes classically involved in TNF and downstream nuclear factor kappa-light-chain-enhancer of activated B cells (NF-κB) signaling, including *Rnf31*. *Rnf31* encodes for HOIL-1-interacting protein (HOIP), the catalytic subunit of the linear ubiquitin chain assembly complex (LUBAC), which also includes SHARPIN and HOIL-1L, encoded by *Sharpin* and *Rbck1* respectively (Haas *et al*, 2009; Tokunaga *et al*, 2011). LUBAC is an E3 ubiquitin ligase capable of forming regulatory N-terminal methionine linked ubiquitin chains, also referred to as linear ubiquitination. LUBAC is required for full TNF/TNF receptor-1 (TNFR1)-mediated gene induction (Haas *et al.*, 2009), and to prevent TNF/TNFR1-induced cell death (Gerlach *et al*, 2011; Tokunaga *et al.*, 2011). Previous work in multiple models supports pro-tumorigenic and anti-apoptotic roles for HOIP in other signaling pathways, with recent studies showing positive effects on tumor cell proliferation (Zhu *et al*, 2014), viability (Yang *et al*, 2014; Zhu *et al*, 2016), and resistance to chemotherapy (MacKay *et al*, 2014; Ruiz *et al*, 2019). In light of these findings, we investigated HOIP in the context of anti-tumor immunity. Here, we show that tumor HOIP limits the anti-tumor activity of both $CD8^+$ T cells and NK cells through protection against the apoptotic effects of TNF in combination with IFN-γ.

RESULTS AND DISCUSSION

HOIP-deficient melanoma cells exhibit increased susceptibility to NK and $CD8^+$ T cell-mediated killing

Our previous CRISPR/Cas9 screen demonstrated that B16-F10 tumor cells lacking genes associated with IFN-γ signaling and antigen processing/presentation were depleted upon NK cell-mediated killing (Freeman *et al*., 2019). Genes associated with TNF and downstream NF-κB signaling were also significantly depleted (**Figure 1A**), including two components of LUBAC: *Rnf31* and *Rbck1* (**Figure 1B**). To rigorously validate these findings, we performed internally controlled competition assays with purified primary mouse NK cells using an equal mixture of sgControl ($mCherry^+$) and sg*Rnf31* ($mCherry^-$) B16-F10 ova tumor cells engineered using CRISPR/Cas9 (**Figure 1C**). sg*Rnf31* tumor cells, which lack HOIP, were significantly depleted after NK cell co-culture (**Figure 1D**). This increased sensitivity to NK cell killing was not a result of altered MHC-I expression on sg*Rnf31* cells after IFN-γ exposure, and was not due to differences in basal proliferation (**Figures EV1A** and **EV1B**).

A role for HOIP in tumor immune evasion is further supported by the identification of *Rnf31* in previous CRISPR/Cas9 screens investigating tumor cell resistance to cytotoxic T cell-mediated killing (Manguso *et al*, 2017; Pan *et al*, 2018). A comparison of the depleted genes from an *in vitro* genome-wide CRISPR/Cas9 screen performed in B16-F10 ova-expressing cells applying OT-I $CD8^+$ T cell

immune pressure (Pan *et al.*, 2018), with the depleted genes from our screen applying NK cell pressure (Freeman *et al.*, 2019), highlighted *Rnf31* and *Rbck1* as potent protectors of both NK cell- and CD8$^+$ T cell-mediated killing (**Figures 1E** and **1F**). Again, we validated this finding by performing internally controlled competition assays with activated OT-I CD8$^+$ T cells using IFN-γ pre-treated sgControl and sg*Rnf31* B16-F10 ova tumor cells, and observed a significant depletion of sg*Rnf31* cells (**Figure 1G**). Together, these data identify, in an unbiased manner, that HOIP is a key regulator of the sensitivity of B16-F10 melanoma cells to killing by both NK cells and CD8$^+$ T cells.

HOIP-deficient melanoma cells exhibit increased sensitivity to combined TNF and IFN-γ

Several reports have established a role for HOIP and linear ubiquitination in protection against TNF-induced cell death (Peltzer *et al*, 2014; Tang *et al*, 2018), however, the majority of these studies have focussed on cells and tissues from non-tumor origins. In the absence of HOIP, caspase 8-mediated apoptosis can be activated by TNF through the formation of the death-inducing Complex II, which is generally associated with impaired NF-κB activation (Haas *et al.*, 2009). Therefore, we next sought to determine if TNF produced and secreted by NK and CD8$^+$ T cells mediated the depletion of sg*Rnf31* B16-F10 ova cells in our competition assays through TNF-induced cell death. The presence of both TNF and IFN-γ within co-culture supernatants prompted us to examine both single and combined effects of TNF and IFN-γ using recombinant cytokines (**Figures EV2A** and **EV2B**). To our surprise, no obvious differences were observed with TNF treatment as a single agent, however, we observed significant depletion of sg*Rnf31* B16-F10 ova tumor cells when treated simultaneously with TNF and IFN-γ (**Figure 2A**). Intriguingly, this effect was observed only when TNF and IFN-γ were combined at the same time and could not be reproduced by prior treatment with the opposing cytokine (**Figure EV2C**). To confirm this result, we performed a genome-wide CRISPR/Cas9 screen using B16-F10 tumor cells to identify the genes depleted after extended culture with recombinant TNF and IFN-γ. Given the previous finding, we hypothesized that multiple LUBAC components would protect against death induced by TNF in combination with IFN-γ. In support of this, *Rnf31* and *Rbck1* (HOIL-1) were among the top significantly depleted genes (**Figures 2B** and **2C**; **Dataset EV1**). Accordingly, biological process gene ontology (GO) analysis of the top significantly depleted genes confirmed the involvement of genes implicated in positive regulation of ubiquitin-protein transferase activity (**Figure 2D**), suggesting that loss of LUBAC activity sensitizes B16-F10 tumor cells to TNF and IFN-γ. Separate comparisons of the depleted genes from this screen with those from our NK cell (Freeman *et al.*, 2019) and the OT-I T cell (Pan *et al.*, 2018) CRISPR/Cas9 screens revealed that *Rnf31* is among the top shared significant genes (**Figures 2E** and **2F)**, suggesting that *Rnf31* potently protects against the combined effect of TNF and IFN-γ co-secreted from both NK and CD8$^+$ T cells. In line

with this, depletion of sg*Rnf31* B16-F10 ova tumor cells in the presence of supernatant derived from a separate OT-I/B16-F10 ova co-culture was rescued when TNF and IFN-γ were neutralized (**Figure EV2D**).

We also validated this observation using A375 human melanoma cells, which harbor the common melanoma-associated $BRAF^{V600E}$ mutation. We directly assessed recombinant cytokine-induced cell death using propidium iodide (PI) staining of sgControl and sg*RNF31* A375 cells engineered using CRISPR/Cas9 (**Figure 2G**). sg*RNF31* A375 tumor cells exhibited increased sensitivity to TNF as a single agent, however, this effect was significantly increased when IFN-γ was also present (**Figure 2H**). Again, this effect was independent of any effects on basal proliferation (**Figure EV2E**). Together, these data demonstrate that tumor expressed HOIP protects mouse and human melanoma cells from combined TNF and IFN-γ-induced cell death. These findings add to the body of evidence that HOIP possesses broader influence on cell death machinery and pathways other than exclusively driving TNF-induced NF-κB activity and inhibiting caspase 8-mediated apoptosis (MacKay *et al.*, 2014; Zhu *et al.*, 2016), and suggests that tumor cells may have evolved to possess additional mechanisms involving HOIP activity to evade cell death. Our findings also challenge the current dogma involving induction of Complex I/II activity solely by TNF and highlights the combinatorial effects with IFN-γ, which is particularly important during anti-tumor immune responses that engage NK cells and $CD8^+$ T cells, which both co-secrete these cytokines. Indeed, the physiological relevance of TNF and IFN-γ synergy has been historically highlighted (Vilcek, 2009), but has been largely overlooked in recent studies investigating anti-tumor responses involving $CD8^+$ T cell-secreted cytokines.

While the cytotoxic effects of TNF have been known for some time (Schulze-Osthoff *et al*, 1998), the contribution of TNF to anti-tumor immunity and response to immunotherapy is only now being appreciated (Kearney *et al*, 2018). As a result, strategies to lower tumor sensitivity to TNF during immunotherapy is an active area of research (Kearney *et al*, 2017; Michie *et al*, 2019; Vredevoogd *et al*, 2019). A recent study utilizing similar genetic screening in human melanoma cells subjected to cytotoxic T cell immune pressure identified several components of TNFR1 Complex I/II as important mediators of caspase-8-dependent killing by $CD8^+$ T cell-derived TNF, including *TRAF2* and *BIRC2* (Vredevoogd *et al.*, 2019). Interestingly, *RNF31* was not among the top depleted hits, most likely due to this screen being performed in IFN-γ receptor 1-deficient melanoma cells. This finding highlights the importance of IFN-γ signaling in conjunction with TNF during the apoptotic phenotype observed with HOIP-deficiency in our study. Taken more broadly, this discrepancy proposes a model where specific components of Complex I may protect tumor cells from TNF-induced apoptosis, depending on the presence or absence of proficient IFN-γ signaling.

Although not formally assessed in our study, our genetic screening results thus far also suggest a role for *Rbck1* as a regulator of cytotoxic lymphocyte killing through combined TNF and IFN-γ. *Rbck1* encodes for another component of LUBAC, heme-oxidized iron-responsive element-binding protein 2 ubiquitin ligase-1 (HOIL-1), which is essential for complex assembly and stability within TNF Complex I (Peltzer *et al*, 2018). Similar mechanisms for HOIP and HOIL-1 in moderating the sensitivity of tumor cells to cytokines may be at play, which involve disruption of proficient LUBAC activity and linear ubiquitin chain formation within Complex I. Destabilization of other LUBAC complex members has previously been reported upon deletion of single components (MacKay *et al.*, 2014; Tokunaga *et al.*, 2011). Interestingly, the remaining component of LUBAC, *Sharpin*, was absent from our significantly depleted screen hits. However, this is consistent with previous work which has shown that HOIP and HOIL-1 are sufficient to form linear ubiquitin chains (Smit *et al*, 2012), and that mutation of *Sharpin* has less pronounced effects than loss of HOIL-1 or HOIP *in vivo* (Peltzer *et al.*, 2018; Peltzer *et al.*, 2014; Rickard *et al*, 2014).

Combined TNF and IFN-γ induces transcription-dependent apoptosis in HOIP-deficient cells that requires both intrinsic and extrinsic apoptotic machinery

We next assessed the cell death pathway involved in the enhanced death of HOIP-deficient B16-F10 tumor cells treated with TNF and IFN-γ. A significant proportion of overnight TNF and IFN-γ-induced cell death of sg*Rnf31* cells was inhibited in the presence of the pan caspase inhibitor, QVD-OPh (**Figure 3A)**, suggesting caspase-dependent apoptosis. This apoptotic cell death was confirmed by Western blot analyses, with caspase-3 cleavage observed in sg*Rnf31* cells treated with combined TNF and IFN-γ (**Figure 3B**, lane 20). sg*Rnf31* cells treated with TNF alone also exhibited evidence of caspase-3 cleavage (**Figure 3B**, lane 8), however, to a lesser extent which additionally failed to translate into confirmed cell death assessed by PI uptake (**Figure EV3A)**. We also observed caspase-8 cleavage in sg*Rnf31* cells treated with combined TNF and IFN-γ (**Figure 3B**, lane 20). Again, sg*Rnf31* cells treated with TNF alone exhibited evidence of caspase-8 cleavage (**Figure 3B**, lane 8), but to a lesser extent. As expected, caspase-8/3 cleavage was absent in sgControl cells treated with TNF alone (**Figure 3B**, lanes 3-5), or combined TNF and IFN-γ (**Figure 3B**, lanes 15-17), and in both sgControl and *sgRnf31* cells treated with IFN-γ alone (**Figure 3B**, lanes 9-14). Together, these data demonstrate that HOIP inhibits caspase-dependent apoptosis induced by combined TNF and IFN-γ.

To impartially uncover factors involved in driving the enhanced cell death and caspase activity, we next performed a genome-wide CRISPR/Cas9 screen using sg*Rnf31* B16-F10 tumor cells to identify genes that, when lost, conferred resistance to killing by TNF and IFN-γ (**Figure 3C**). Consistent with our data showing that a combined TNF and IFN-γ stimulus is required to induce apoptosis in HOIP-deficient cells, genes required for classical IFN-γ (*Ifngr1, Ifngr2, Jak1, Jak2,* and *Stat1*) and TNF signaling (*Tnfrsf1a, Ripk1, Tradd, Chuk, Ikbkb*, and *Rela*) were both significantly enriched in this

screen (**Figures 3D** and **3E**; **Dataset EV2**). This was further supported by biological process GO term analysis of the top significantly enriched genes which revealed several terms associated with cytokine mediated signaling and signal transduction (**Figure 3F**). Additionally, the enrichment of *Fadd* (**Figure EV3B**), a gene involved in the formation of the death-inducing signaling complex (DISC) - which is known to regulate activity of the initiator caspase, caspase-8 (Micheau & Tschopp, 2003), suggested a contribution of classical extrinsic apoptotic machinery. Furthermore, Bid, a pro-apoptotic member of the Bcl-2 family of proteins, which is activated by the extrinsic apoptosis effector, caspase-8 (Li *et al*, 1998), and which in turn activates mitochondrial Bax/Bak to induce intrinsic apoptosis (Korsmeyer *et al*, 2000), was also significantly enriched in sg*Rnf31* cells upon combined TNF and IFN-γ treatment (**Figure 3C**; **Dataset EV2**). Indeed, combined TNF and IFN-γ-induced apoptosis of sg*Rnf31* B16-F10 tumor cells was dependent on the presence of both Bax and Bak (**Figures EV3C** and **EV3D**). To validate these findings, we engineered sg*Rnf31* B16-F10 tumor cells individually lacking *Stat1, Casp8, Bid,* and *Rela* using CRISPR/Cas9 (**Figure EV3E**). We confirmed dependence on these genes during apoptosis of sg*Rnf31* B16-F10 tumor cells treated with TNF and IFN-γ (**Figure 3G**), with consistent levels of protection observed relative to those identified in our CRISPR/Cas9 screen. These findings demonstrate that the observed cell death was dependent on both the transcriptional activity of signal transducer and activator of transcription-1 (STAT1) and p65 (encoded by *Rela*), which converge on the classical apoptosis-inducing molecules, caspase-8, Bid, and Bax/Bak. Taken together, these data demonstrate that HOIP protects tumor cells from a transcription-dependent form of apoptosis arising from TNF and IFN-γ synergy that requires components of both intrinsic and extrinsic apoptotic machinery.

Although IFN-γ itself is not generally associated with cytotoxicity, previous work has highlighted the essential role of IFN-γ signaling during apoptosis arising from TNF and IFN-γ synergy in tumor cells (Suk *et al*, 2001). This synergy was recently highlighted in the context of tissue damage associated with cytokine shock during severe acute respiratory syndrome coronavirus 2 (SARS-CoV-2) infection (Karki *et al*, 2021), where combined TNF and IFN-γ resulted in induction of nitric oxide (NO) and the simultaneous downstream activation of several apoptotic pathways, coined PANoptosis, in bone-marrow-derived macrophages. In contrast to this study, we failed to inhibit the enhanced apoptotic response observed in HOIP deficient cells treated with combined TNF and IFN-γ in the presence of the inducible NO synthase inhibitor, 1400W (**Figure EV3F**), suggesting that induction of apoptosis in our model is independent of NO activity. Similar to our findings, previous studies investigating TNF and IFN-γ synergy have demonstrated dependence on STAT1 (Karki *et al.*, 2021; Suk *et al.*, 2001), linking STAT1-mediated responses to apoptosis. Our study supports this association and suggests that tumors may exploit HOIP activity to inhibit downstream apoptosis linked to STAT1 and NF-κB activity in the presence of combined TNF and IFN-γ. STAT1 was recently shown to undergo linear ubiquitination modifications by HOIP, which limited type-I IFN anti-viral responses mediated

through IFN-α/β receptor 2 (Zuo *et al*, 2020). Although our study lacks explicit delineation of the molecular processes involving the genes identified in our cytokine resistance CRISPR/Cas9 screen performed in HOIP-deficient tumor cells, comparable inhibitory mechanisms by HOIP may be occurring in our models, involving pro-apoptotic STAT1 responses mediated through IFN-γ in the presence of TNF. The dependence of classical NF-κB signaling genes and *Rela* itself during our apoptotic phenotype also intriguingly mirrors that of previous reports which demonstrate the complex nature of NF-κB signaling during tumor cell apoptosis (Perkins & Gilmore, 2006; Ryan *et al*, 2000).

Pharmacological inhibition of HOIP sensitizes tumor cells to combined TNF and IFN-γ induced apoptosis *in vitro*

The emergence of data supporting the pro-tumorigenic and anti-apoptotic role of LUBAC has resulted in the recent development of small-molecule inhibitors of HOIP, which reduce linear ubiquitination, canonical NF-κB signaling, and increase TNF-induced apoptosis in pre-clinical studies (Katsuya *et al*, 2019; Oikawa *et al*, 2020). We therefore sought to determine if we could phenocopy genetic deletion of HOIP with pharmacological inhibition using a recently developed HOIP inhibitor (HOIPIN), HOIPIN-1 (Katsuya *et al*, 2018), which has demonstrated superior specificity compared to previously used LUBAC inhibitors (Oikawa *et al.*, 2020; Sakamoto *et al*, 2015; Strickson *et al*, 2013). Strikingly, pre-treatment with HOIPIN-1, while not intrinsically toxic, significantly sensitized otherwise resistant parental B16-F10 tumor cells to apoptosis induced by recombinant TNF and IFN-γ (**Figure 4A**). To confirm this observation on tumor cell death in a more physiological setting, we repeated this assay using supernatant from OT-I T cell/B16-F10 ova co-cultures in place of recombinant cytokine. HOIPIN-1 pre-treatment similarly sensitized B16-F10 tumor cells to co-culture supernatants derived from various effector to target (E:T) ratios (**Figure 4B**). To rule out a direct effect of HOIPIN-1 treatment on T cell function upon antigen recognition, we pre-treated OT-I T cells with HOIPIN-1 and then co-cultured them with B16-F10 ova cells. We observed no differences in the levels of TNF and IFN-γ secreted in co-culture supernatants from HOIPIN-1 pre-treated OT-I T cells compared to vehicle pre-treated (**Figure EV4A**), suggesting that HOIP inhibition does not deleteriously affect cytokine secretion from activated $CD8^+$ T cells. Taken together, these data demonstrate that pharmacological inhibition of HOIP can sensitize tumor cells to apoptosis induced by combined TNF and IFN-γ. In addition to mouse melanoma cells, we also demonstrated increased sensitivity to apoptosis induced by TNF and IFN-γ in parental A375 human melanoma cells following HOIPIN-1 pre-treatment (**Figure 4C**). This observation also extended to HeLa human cervical adenocarcinoma cells (**Figure EV4B**), suggesting that the effect of HOIP inhibition is not restricted to melanoma cells. Indeed, the tumor immune estimation resource (TIMER) (Li *et al*, 2017), indicated that *RNF31* expression is significantly upregulated in tumors compared to normal tissue for the majority of the Cancer Genome Atlas (TCGA) cancer types where normal tissue data is available (13/17 TCGA cancer types) (**Figure EV4C**). In light of our findings, this suggests that multiple cancer types may

upregulate expression of HOIP to facilitate evasion from immune mediated apoptosis, which may be overcome by pharmacological HOIP inhibition depending on the level and activity of immune cell infiltrate. Importantly, TNF and IFN-γ production and release is not limited to innate and adaptive cytotoxic lymphocytes but extends to a myriad of immune cells which can also be present and active within the tumor microenvironment.

HOIP-deficient tumors exhibit enhanced OT-I-mediated control *in vivo*

In the absence of a HOIPIN that is established for systemic *in vivo* treatment of mice, we utilized an adoptive cell therapy model using tumors with genetic deletion of *Rnf31* to test whether HOIP inhibition may be clinically feasible (**Figure 5A**). Consistent with our *in vitro* data, established sg*Rnf31* B16-F10 ova tumors implanted subcutaneously into C57BL/6J mice were controlled significantly better by adoptively transferred pre-activated OT-I $CD8^+$ T cells compared to wild-type B16-F10 ova tumors (**Figures 5B** and **EV5**), which importantly translated into significantly extended overall survival of the mice (**Figure 5C**). These data provide imperative proof-of-principle that HOIP indeed influences responses *in vivo*, and suggests that inhibiting HOIP activity within tumors may enhance their response to anti-tumor immune effector cells, such as $CD8^+$ T cells.

Our findings provide a mechanistic foundation and rationale for the further investigation of pharmacological HOIP inhibition in the context of immunotherapeutic settings where TNF and IFN-γ levels are elevated. Our *in vivo* therapy model demonstrating that genetic deletion of HOIP can sensitize tumors to control by immune effector cells supports the notion that future exploration of suitable therapeutic approaches to modulate LUBAC activity is warranted. A recently developed derivative of HOIPIN-1, HOIPIN-8, exhibited greater potency than HOIPIN-1 in pre-clinical studies and may be a suitable lead for future development in this field (Katsuya *et al.*, 2019; Oikawa *et al.*, 2020). HOIPIN-8 exhibited accelerated TNF-induced apoptosis of a human tumor cell line in the presence of protein synthesis inhibition using cyclohexamide, compared to HOIPIN-1 *in vitro* (Oikawa *et al.*, 2020). Notably, our results utilizing HOIPIN-1 were performed in the absence of such inhibition and thus represents a feasible strategy to harness a transcription-dependent form of apoptosis mediated through combined TNF and IFN-γ. Additionally, our HOIPIN-1 experiments assessed tumor cell killing by cytokine in the absence of any direct lymphocyte-tumor conjugation, which may have positive implications for TNF and IFN-γ induced 'bystander' killing of antigen-negative tumor cells that have downregulated essential antigen presentation proteins to evade T cell attack during immunotherapy (Restifo *et al*, 1996; Sade-Feldman *et al*, 2017).

Conclusion

Taken together, we unbiasedly identify a role for tumor-expressed HOIP, the catalytic component of LUBAC, in limiting anti-tumor immunity by protecting against the combined apoptotic effects of TNF and IFN-γ, released by activated NK cells and $CD8^+$ T cells. Mechanistically, components of

both intrinsic and extrinsic apoptotic machinery are harnessed by TNF and IFN-γ under conditions of reduced HOIP expression. In addition, pharmacological HOIP inhibition resulted in augmented sensitivity of intrinsically resistant melanoma cells to combined TNF and IFN-γ-mediated apoptosis. Our collective findings not only contribute to the growing body of evidence describing the importance of pro-inflammatory cytokines during anti-tumor immune responses, but also highlights HOIP as a potential combinatorial target to harness the apoptotic activity of combined TNF and IFN-γ to ultimately augment the killing capacity of both adaptive and innate cytotoxic lymphocytes during current and future immunotherapeutic interventions.

MATERIALS AND METHODS

Cell lines and primary cell cultures

B16-F10 (RRID:CVCL_0159) mouse melanoma cells, originally from American Type Culture Collection, and its ova-expressing derivative were cultured in DMEM supplemented with 10% FBS and incubated at 37°C with 10% CO_2. A375 (RRID:CVCL_0132) human melanoma cells were provided by the Molecular Oncology Laboratory (Peter MacCallum Cancer Centre Research Division). HeLa (RRID:CVCL_0030) human cervical adenocarcinoma cells were provided by the Organogenesis and Cancer Laboratory (Peter MacCallum Cancer Centre Research Division). A375 and HeLa cells were cultured in a similar fashion to B16-F10 cells. Cell lines were verified to be *Mycoplasma*-negative by external PCR analysis prior to the commencement of any experiments.

Primary mouse NK cells were isolated from splenocytes of 8 to 12 week old female C57BL/6J mice using the EasySep Mouse NK Cell Isolation Kit (Stemcell Technologies; Cat:19855) according to the manufacturer's instructions. NK cells were cultured in RPMI medium supplemented with 10% FBS, penicillin/streptomycin, L-glutamine, non-essential amino acids, sodium pyruvate, HEPES, β_2-mercaptoethanol, and 1000 IU/mL recombinant human interleukin-2 (IL-2) (Roche; Cat:R20-6019) and incubated at 37°C with 5% CO_2. Purified mouse NK were used 6 days after culture. Splenocytes of 8 to 12 week old C57BL/6J.OT-I mice were activated with 10 ng/mL of the $ova_{257-264}$ peptide, SIINFEKL (Auspep; Cat:2711), for 3 days. OT-I cells were cultured in the same conditions as NK cells but with 100 IU/mL recombinant human IL-2. Activated OT-I cells were used 4 days after culture (*in vivo*) or 5-7 days after culture (*in vitro*).

Animals and *in vivo* experiments

All animal procedures were performed in accordance with the National Health and Medical Research Council (NHMRC) *Australian Code for the care and use of animals for scientific purposes 8th edition (2013)* and with approval from the Peter MacCallum Animal Experimentation Ethics Committee. C57BL/6J mice were purchased from the Walter and Eliza Hall Institute (WEHI) of Medical Research

and C57BL/6J.OT-I transgenic mice were bred in house. All experimental animals were housed in the Peter MacCallum Cancer Centre Animal Core Facility, a temperature and light controlled, pathogen-free environment with food and water provided *ad libitum*.

For *in vivo* experiments, female 12-week old C57BL/6J mice were subcutaneously injected with 2×10^5 wild-type or sg*Rnf31* B16-F10 ova cells in the right flank and left to establish for 7 days. Groups containing similar tumor sizes were left untreated or intravenously injected with 2.5×10^6 4-day cultured OT-I T cells on days 9 and 12 post tumor inoculation. Tumor area was measured 3 times a week using digital callipers in a non-blinded fashion. Mice were euthanized if they exhibited symptoms of distress or when tumor size reached ethical endpoint of 200 mm^2.

Generation of CRISPR/Cas9-edited cell lines

For validation experiments, 2×10^5 viable B16-F10 ova or A375 tumor cells were added to a ribonucleoprotein (RNP) complex consisting of recombinant Cas9 nuclease (Integrated DNA Technologies; Cat:1081059) and 2 sgRNA guides (purchased from Synthego) targeting the gene of interest and electroporated using the Amaxa 4D-Nucleofector System (Lonza). Mouse sgRNA sequences were as follows:

sgControl: (1) AAGCACAAGAACGGTCCGCC, (2) AAAAAGTCCGCGATTACGTC;

sg*Rnf31*: (1) GAACTATGAGTTGTTGGACG, (2) GATGGATTGAGTTTCCCCGA;

sg*Stat1*: (1) GGATAGACGCCCAGCCACTG, (2) TGTGATGTTAGATAAACAGA;

sg*Bid*: (1) CCACAACATCCAGCCCACAC, (2) GCCAGCCGCTCCTTCAACCA;

sg*Rela*: (1) TATCAAAAATCGGATGTGAG, (2) GATTCCGCTATAAATGCGAG;

sg*Casp8*: (1) ATGATCAGACAGTATCCCCG, (2) CAAGAAGCAGGAGACCATCG;

sg*Bax*: (1) GGACACGGACTCCCCCCGAG, (2) GTTTCATCCAGGATCGAGCA;

sg*Bak1*: (1) GGAACTCTGTGTCGTAGCGC, (2) GCAGGAGGCTCTTACCAGAA.

Human sgRNA sequences were as follows:

sgControl: (1) AAAAAGCTTCCGCCTGATGG, (2) AAAACAGGACGATGTGCGGC;

sg*RNF31*: (1) CCACCGTGCTGCGAAAGACA, (2) GGATCATGCTCACTAGCTGG.

Proteins, reagents, and antibodies

The following recombinant cytokines were purchased from PeproTech: mouse TNF (Cat:315-01A), mouse IFN-γ (Cat:315-05), human TNF (Cat:300-01A), human IFN-γ (Cat:300-02). PI was purchased from Thermo Fisher Scientific (Cat:P1304MP). QVD-OPh was purchased from Merck Millipore-

Calbiochem (Cat:551476). HOIPIN-1 was purchased from Glixx Laboratories (Cat:GLXC-22001) and was dissolved in dimethyl sulfoxide. Anti-mouse neutralizing α-TNF antibody was purchased from Biolegend (Cat:506325). Anti-mouse neutralizing α-IFN-γ antibody was purchased from BioXCell (Cat:BE0312).

The following primary antibodies used for Western blot analysis were purchased from Abcam, Cell Signaling Technology (CST), Merck Millipore, or Sigma Aldrich: HOIP (Abcam; Cat:ab46322), STAT1 (Merck Millipore; Cat:06-501), p65 (Abcam; Cat:ab7970), Caspase-3 (CST; Cat:9665), Cleaved caspase-3 (Asp175) (CST; Cat:9664), β-Actin (Sigma Alrdich; Cat:A2228), Caspase-8 (CST; Cat:4927), Cleaved caspase-8 (Asp387) (CST; Cat:8592), Bak (Sigma Aldrich; Cat:B5897). Bax and Bid primary antibodies were both gifts from Vivien Sutton, originally generated in-house at WEHI (Czabotar *et al*, 2013; Kaufmann *et al*, 2007). The following secondary antibodies used for Western blot analysis were purchased from Agilent Dako or Invitrogen: swine anti-rabbit IgG/HRP (Agilent Dako; Cat:P0217), rabbit anti-mouse IgG/HRP (Agilent Dako; Cat:P0260), rabbit anti-rat IgG (H+L) (Invitrogen; Cat:61-9520).

Combined IFN-γ/TNF CRISPR/Cas9 screens

For the B16-F10 dropout screen, Cas9-expressing B16-F10 cells were transduced with lentivirus containing the genome-scale mouse CRISPR library, Brie, as previously described (Freeman *et al.*, 2019). Brie-transduced B16-F10 Cas9 cells were then cultured in the presence of recombinant TNF/IFN-γ (both 10 ng/mL) for 7 days. An untreated control sample was cultured alongside the treated cells was used for comparison. For the sg*Rnf31* resistance screen, sg*Rnf31* B16-F10 cells, originally created using RNP-based CRISPR/Cas9, were transduced to stably express mCherry-Cas9 using the FUCas9Cherry plasmid (Addgene; Plasmid#70182) and then transduced with lentivirus containing Brie, as previously described (Freeman *et al.*, 2019). Brie-transduced sg*Rnf31* B16-F10 Cas9 cells were then subjected to 3 successive overnight cultures with recombinant TNF/IFN-γ (both 10 ng/mL), with washing and recovery after each treatment. An untreated control sample was again used for comparison. Genomic DNA extraction, sgRNA sequence amplification by PCR, next generation sequencing, Model-based Analysis of Genome-wide CRISPR/Cas9 Knockout (MAGeCK) and visualization were performed for both screens as previously described (Freeman *et al.*, 2019). The CRISPR/Cas9 screen datasets generated during this study are included as Expanded View material (**Datasets EV1** and **EV2**).

***In vitro* assays**

For competition assays, sgControl or *sgRnf31* B16-F10 ova cells were equally mixed, plated, and allowed to adhere. For mouse NK competition assays, B16-F10 ova tumor cells were co-cultured with NK cells at a 1:1 E:T ratio for 72 hours. For OT-I competition assays, B16-F10 ova cells were pre-treated overnight with 1 ng/mL IFN-γ to upregulate MHC-I expression, and then co-cultured with OT-

I T cells at a 1:4 E:T ratio for 72 hours. For recombinant cytokine competition assays, mixed B16-F10 ova cells were cultured in the presence of TNF (10 ng/mL), IFN-γ (10 ng/mL) or TNF/IFN-γ (both 10 ng/mL) for 48 hours. Technical triplicate samples were run on a LSRFortessa X20 flow cytometer with FACSDiva software (BD Biosciences) and the proportion of sgControl cells of viable tumor cells was assessed based on mCherry expression using FlowJo software (TreeStar, v10).

For PI assays involving recombinant cytokine and supernatant, percentage of dead cells within technical triplicate wells was assessed by the addition of 1.5 μM PI. Samples were directly run on a LSRII flow cytometer with FACSDiva software (BD Biosciences) and the proportion and gating of dead cells was based on untreated samples using FlowJo software (TreeStar, v10).

To evaluate the induction of MHC-I on sgControl and sg*Rnf31* B16-F10 ova cells, cells were left untreated or cultured in the presence of 5 ng/mL IFN-γ for 18 hours in technical triplicate determinations. Cells were washed in 2% FBS/PBS and stained with diluted anti-mouse H-2K^b-PE (BD Biosciences; Cat:553570) for 30 min at 4°C. Stained cells were washed twice and then run on a LSRII flow cytometer with FACSDiva software (BD Biosciences). MFI fold change was calculated from untreated and IFN-γ-treated samples using FlowJo software (TreeStar, v10). To assess proliferation, 1×10^4 sgControl or sg*Rnf31* B16-F10 ova cells were plated in separate wells and counted for the following 4 days. For A375 cells, 5×10^4 cells were initially plated.

Cytokine detection

The concentrations of TNF and IFN-γ in supernatants from NK cell and OT-I T cell co-culture assays after 24 hours were determined using a cytometric bead array Mouse Inflammation Kit (BD Biosciences; Cat:552364), according to the manufacturer's instructions. Samples were run on a FACSVerse flow cytometer (BD Biosciences) and data were analyzed using FCAP Array software (BD Biosciences, v3).

Western blot analysis

Viable cells were directly lysed in ice cold SDS loading buffer (Tris-Cl, SDS, bromophenol blue, glycerol, and β_2-mercaptoethanol, pH 6.8), thoroughly mixed, boiled at 95°C, and centrifuged at 1×10^4 g for 10 min at 4°C. Equal amounts of lysates were loaded into Tris-glycine gels and proteins were separated using SDS-polyacrylamide gel electrophoresis. Separated proteins were wet transferred onto Immobolin-P PVDF membranes (Sigma Aldrich; Cat:IPVH00010) and blocked with 5% skim milk in 0.1% PBS-Tween for 1 hour at room temperature before overnight incubation with primary antibodies at 4°C. Membranes were then incubated with corresponding secondary antibodies

for 1 hour at room temperature and visualized on an iBright FL1500 Imaging System (Thermo Fisher Scientific) using Amersham ECL Western Blotting Detection Reagents (Sigma Aldrich; Cat:RPN2106) or Chemiluminescent Peroxidase Substrate-3 (Sigma Aldrich; Cat:CPS3500-KT).

Statistical analysis

Statistical details of experiments can be found in the figure legends, where n represents the number of biological replicates performed. With the exception of CRISPR/Cas9 screen data, GraphPad Prism 8 software was used to determine statistical significance using either an unpaired Student's *t*-test or a Log-rank test. A Wilcoxon test was used to determine statistical significance for TCGA data. Where appropriate, pooled data are represented as mean ± SEM, and differences were considered significant when $p < 0.05$.

ACKNOWLEDGEMENTS

For their resources and contributions to this work, we acknowledge the Australian Cancer Research Foundation and TCGA Research Network. We also acknowledge the following Peter MacCallum Cancer Centre Research Division cores: The Victorian Centre for Functional Genomics, Molecular Genomics, Flow Cytometry Facility, and Animal Facility. We thank Shirley Liu and Peng Jiang for kindly providing raw OT-I B16-F10 ova CRISPR/Cas9 screen data, Vivien Sutton for supply of OT-I mice, and James Vince and colleagues at WEHI for helpful discussions.

A.J.F. was supported by scholarships from Australian Commonwealth Government, Steer North Australia, and the Peter MacCallum Cancer Foundation. C.J.K. was supported by a NHMRC Early Career Fellowship. J.O. was supported by NHMRC (1139626) and National Breast Cancer Foundation (IIRS-18-151) project grants.

AUTHOR CONTRIBUTIONS

Conceptualization: A.J.F.; Methodology: A.J.F., S.J.V., C.J.K., and J.O.; Investigation: A.J.F., J.M., and K.M.R.; Visualization: A.J.F.; Writing – Original Draft: A.J.F.; Writing – Review & Editing: A.J.F., C.J.K., J.S. and J.O.; Funding Acquisition: J.O.; Supervision: C.J.K. and J.O. All authors read and approved the final manuscript.

CONFLICT OF INTEREST

The authors declare no competing interests.

DATA AVAILABILITY

No primary datasets have been deposited to a public database.

REFERENCES

Czabotar PE, Westphal D, Dewson G, Ma S, Hockings C, Fairlie WD, Lee EF, Yao S, Robin AY, Smith BJ *et al* (2013) Bax crystal structures reveal how BH3 domains activate Bax and nucleate its oligomerization to induce apoptosis. *Cell* 152: 519-531

Freeman AJ, Vervoort SJ, Ramsbottom KM, Kelly MJ, Michie J, Pijpers L, Johnstone RW, Kearney CJ, Oliaro J (2019) Natural killer cells suppress T cell-associated tumor immune evasion. *Cell Rep* 28: 2784-2794.e2785

Gerlach B, Cordier SM, Schmukle AC, Emmerich CH, Rieser E, Haas TL, Webb AI, Rickard JA, Anderton H, Wong WWL *et al* (2011) Linear ubiquitination prevents inflammation and regulates immune signalling. *Nature* 471: 591-596

Haas TL, Emmerich CH, Gerlach B, Schmukle AC, Cordier SM, Rieser E, Feltham R, Vince J, Warnken U, Wenger T *et al* (2009) Recruitment of the linear ubiquitin chain assembly complex stabilizes the TNF-R1 signaling complex and is required for TNF-mediated gene induction. *Mol Cell* 36: 831-844

Karki R, Sharma BR, Tuladhar S, Williams EP, Zalduondo L, Samir P, Zheng M, Sundaram B, Banoth B, Malireddi RKS *et al* (2021) Synergism of TNF-α and IFN-γ triggers inflammatory cell death, tissue damage, and mortality in SARS-CoV-2 infection and cytokine shock syndromes. *Cell* 184: 149-168.e117

Katsuya K, Hori Y, Oikawa D, Yamamoto T, Umetani K, Urashima T, Kinoshita T, Ayukawa K, Tokunaga F, Tamaru M (2018) High-throughput screening for linear ubiquitin chain assembly complex (LUBAC) selective inhibitors using homogenous time-resolved fluorescence (HTRF)-based assay system. *SLAS Discov* 23: 1018-1029

Katsuya K, Oikawa D, Iio K, Obika S, Hori Y, Urashima T, Ayukawa K, Tokunaga F (2019) Small-molecule inhibitors of linear ubiquitin chain assembly complex (LUBAC), HOIPINs, suppress NF-kappaB signaling. *Biochem Biophys Res Commun* 509: 700-706

Kaufmann T, Tai L, Ekert PG, Huang DCS, Norris F, Lindemann RK, Johnstone RW, Dixit VM, Strasser A (2007) The BH3-only protein bid is dispensable for DNA damage- and replicative stress-induced apoptosis or cell-cycle arrest. *Cell* 129: 423-433

Kearney CJ, Lalaoui N, Freeman AJ, Ramsbottom KM, Silke J, Oliaro J (2017) PD-L1 and IAPs co-operate to protect tumors from cytotoxic lymphocyte-derived TNF. *Cell Death Differ* 24: 1705-1716

Kearney CJ, Vervoort SJ, Hogg SJ, Ramsbottom KM, Freeman AJ, Lalaoui N, Pijpers L, Michie J, Brown KK, Knight DA *et al* (2018) Tumor immune evasion arises through loss of TNF sensitivity. *Sci Immunol* 3

Korsmeyer SJ, Wei MC, Saito M, Weiler S, Oh KJ, Schlesinger PH (2000) Pro-apoptotic cascade activates BID, which oligomerizes BAK or BAX into pores that result in the release of cytochrome c. *Cell Death Differ* 7: 1166-1173

Li H, Zhu H, Xu CJ, Yuan J (1998) Cleavage of BID by caspase 8 mediates the mitochondrial damage in the Fas pathway of apoptosis. *Cell* 94: 491-501

Li T, Fan J, Wang B, Traugh N, Chen Q, Liu JS, Li B, Liu XS (2017) TIMER: a web server for comprehensive analysis of tumor-infiltrating immune cells. *Cancer Res* 77: e108-e110

MacKay C, Carroll E, Ibrahim AFM, Garg A, Inman GJ, Hay RT, Alpi AF (2014) E3 ubiquitin ligase HOIP attenuates apoptotic cell death induced by cisplatin. *Cancer Res* 74: 2246-2257

Manguso RT, Pope HW, Zimmer MD, Brown FD, Yates KB, Miller BC, Collins NB, Bi K, LaFleur MW, Juneja VR *et al* (2017) In vivo CRISPR screening identifies Ptpn2 as a cancer immunotherapy target. *Nature* 547: 413-418

Maude SL, Teachey DT, Porter DL, Grupp SA (2015) CD19-targeted chimeric antigen receptor T-cell therapy for acute lymphoblastic leukemia. *Blood* 125: 4017-4023

Micheau O, Tschopp J (2003) Induction of TNF receptor I-mediated apoptosis via two sequential signaling complexes. *Cell* 114: 181-190

Michie J, Beavis PA, Freeman AJ, Vervoort SJ, Ramsbottom KM, Narasimhan V, Lelliott EJ, Lalaoui N, Ramsay RG, Johnstone RW *et al* (2019) Antagonism of IAPs enhances CAR T-cell efficacy. *Cancer Immunol Res* 7: 183-192

Oikawa D, Sato Y, Ohtake F, Komakura K, Hanada K, Sugawara K, Terawaki S, Mizukami Y, Phuong HT, Iio K *et al* (2020) Molecular bases for HOIPINs-mediated inhibition of LUBAC and innate immune responses. *Commun Biol* 3: 163

Pan D, Kobayashi A, Jiang P, Ferrari de Andrade L, Tay RE, Luoma AM, Tsoucas D, Qiu X, Lim K, Rao P *et al* (2018) A major chromatin regulator determines resistance of tumor cells to T cell-mediated killing. *Science* 359: 770-775

Peltzer N, Darding M, Montinaro A, Draber P, Draberova H, Kupka S, Rieser E, Fisher A, Hutchinson C, Taraborrelli L *et al* (2018) LUBAC is essential for embryogenesis by preventing cell death and enabling haematopoiesis. *Nature* 557: 112-117

Peltzer N, Rieser E, Taraborrelli L, Draber P, Darding M, Pernaute B, Shimizu Y, Sarr A, Draberova H, Montinaro A *et al* (2014) HOIP deficiency causes embryonic lethality by aberrant TNFR1-mediated endothelial cell death. *Cell Rep* 9: 153-165

Perkins ND, Gilmore TD (2006) Good cop, bad cop: the different faces of NF-kappaB. *Cell Death Differ* 13: 759-772

Restifo NP, Marincola FM, Kawakami Y, Taubenberger J, Yannelli JR, Rosenberg SA (1996) Loss of functional beta 2-microglobulin in metastatic melanomas from five patients receiving immunotherapy. *J Natl Cancer Inst* 88: 100-108

Ribas A, Hamid O, Daud A, Hodi FS, Wolchok JD, Kefford R, Joshua AM, Patnaik A, Hwu WJ, Weber JS *et al* (2016) Association of pembrolizumab with tumor response and survival among patients with advanced melanoma. *JAMA* 315: 1600-1609

Rickard JA, Anderton H, Etemadi N, Nachbur U, Darding M, Peltzer N, Lalaoui N, Lawlor K, Vanyai H, Hall C *et al* (2014) TNFR1-dependent cell death drives inflammation in Sharpin-deficient mice. *eLife* 3

Ruiz EJ, Diefenbacher ME, Nelson JK, Sancho R, Pucci F, Chakraborty A, Moreno P, Annibaldi A, Liccardi G, Encheva V *et al* (2019) LUBAC determines chemotherapy resistance in squamous cell lung cancer. *J Exp Med* 216: 450-465

Ryan KM, Ernst MK, Rice NR, Vousden KH (2000) Role of NF-kappaB in p53-mediated programmed cell death. *Nature* 404: 892-897

Sade-Feldman M, Jiao YJ, Chen JH, Rooney MS, Barzily-Rokni M, Eliane J-P, Bjorgaard SL, Hammond MR, Vitzthum H, Blackmon SM *et al* (2017) Resistance to checkpoint blockade therapy through inactivation of antigen presentation. *Nat Commun* 8: 1136-1136

Sakamoto H, Egashira S, Saito N, Kirisako T, Miller S, Sasaki Y, Matsumoto T, Shimonishi M, Komatsu T, Terai T *et al* (2015) Gliotoxin suppresses NF-κB activation by selectively inhibiting linear ubiquitin chain assembly complex (LUBAC). *ACS Chem Biol* 10: 675-681

Schulze-Osthoff K, Ferrari D, Los M, Wesselborg S, Peter ME (1998) Apoptosis signaling by death receptors. *Eur J Biochem* 254: 439-459

Shi H, Lan J, Yang J (2020) Mechanisms of resistance to checkpoint blockade therapy. *Adv Exp Med Biol* 1248: 83-117

Smit JJ, Monteferrario D, Noordermeer SM, van Dijk WJ, van der Reijden BA, Sixma TK (2012) The E3 ligase HOIP specifies linear ubiquitin chain assembly through its RING-IBR-RING domain and the unique LDD extension. *EMBO J* 31: 3833-3844

Souza-Fonseca-Guimaraes F, Cursons J, Huntington ND (2019) The emergence of natural killer cells as a major target in cancer immunotherapy. *Trends Immunol* 40: 142-158

Strickson S, Campbell DG, Emmerich CH, Knebel A, Plater L, Ritorto M, Shpiro N, Cohen P (2013) The anti-inflammatory drug BAY 11-7082 suppresses the MyD88-dependent signalling network by targeting the ubiquitin system. *Biochem J* 451: 427-437

Suk K, Chang I, Kim YH, Kim S, Kim JY, Kim H, Lee MS (2001) Interferon γ (IFNγ) and tumor necrosis factor α synergism in ME-180 cervical cancer cell apoptosis and necrosis. IFNγ inhibits cytoprotective NF-kappa B through STAT1/IRF-1 pathways. *J Biol Chem* 276: 13153-13159

Tang Y, Tu H, Liu G, Zheng G, Wang M, Li L, Zhao X, Lin X (2018) RNF31 regulates skin homeostasis by protecting epidermal keratinocytes from cell death. *J Immunol* 200: 4117-4124

Tokunaga F, Nakagawa T, Nakahara M, Saeki Y, Taniguchi M, Sakata S, Tanaka K, Nakano H, Iwai K (2011) SHARPIN is a component of the NF-kappaB-activating linear ubiquitin chain assembly complex. *Nature* 471: 633-636

Vilcek J (2009) From IFN to TNF: a journey into realms of lore. *Nat Immunol* 10: 555-557

Vredevoogd DW, Kuilman T, Ligtenberg MA, Boshuizen J, Stecker KE, de Bruijn B, Krijgsman O, Huang X, Kenski JCN, Lacroix R *et al* (2019) Augmenting immunotherapy impact by lowering tumor TNF cytotoxicity threshold. *Cell* 178: 585-599.e515

Yang Y, Schmitz R, Mitala J, Whiting A, Xiao W, Ceribelli M, Wright GW, Zhao H, Yang Y, Xu W *et al* (2014) Essential role of the linear ubiquitin chain assembly complex in lymphoma revealed by rare germline polymorphisms. *Cancer Discov* 4: 480-493

Zhu J, Zhao C, Kharman-Biz A, Zhuang T, Jonsson P, Liang N, Williams C, Lin CY, Qiao Y, Zendehdel K *et al* (2014) The atypical ubiquitin ligase RNF31 stabilizes estrogen receptor alpha and modulates estrogen-stimulated breast cancer cell proliferation. *Oncogene* 33: 4340-4351

Zhu J, Zhao C, Zhuang T, Jonsson P, Sinha I, Williams C, Stromblad S, Dahlman-Wright K (2016) RING finger protein 31 promotes p53 degradation in breast cancer cells. *Oncogene* 35: 1955-1964

Zuo Y, Feng Q, Jin L, Huang F, Miao Y, Liu J, Xu Y, Chen X, Zhang H, Guo T *et al* (2020) Regulation of the linear ubiquitination of STAT1 controls antiviral interferon signaling. *Nat Commun* 11: 1146-1146

FIGURE LEGENDS

Figure 1: HOIP-deficient melanoma cells exhibit increased susceptibility to NK and CD8$^+$ T cell-mediated killing

(A) Summary of top depleted pathways and associated genes from our previous B16-F10 dropout CRISPR/Cas9 screen performed with NK cells; **p < 0.01, ***p < 0.001, ****p < 0.0001, MAGeCK test.

(B) Individual sgRNA count values from (A) for *Rnf31* (left) and *Rbck1* (right); significance assessed using MAGeCK test.

(C) Western blot analysis on whole cell lysates showing HOIP expression for sgControl and sg*Rnf31* B16-F10 ova tumor cells created using CRISPR/Cas9; β-actin was used as a loading control.

(D) Representative flow cytometry plots (left) and pooled data (right) of competition assays with sgControl and sg*Rnf31* B16-F10 ova tumor cells cultured with NK cells for 72 hours; **p < 0.01, Unpaired *t*-test for n = 3 biological replicates. Pooled data are represented as mean ± SEM.

(E) OT-I and NK cell B16-F10 dropout CRISPR/Cas9 screen comparison; significant genes from LUBAC are labelled.

(F) Venn diagram showing the shared top significantly depleted genes from (E); LUBAC components are highlighted; indicated genes were filtered by p < 0.01 and for 3/4 affected sgRNA in both screens.

(G) Representative flow cytometry plots (left) and pooled data (right) of competition assays with IFN-γ (1 ng/mL) pre-treated sgControl and sg*Rnf31* B16-F10 ova tumor cells cultured with OT-I CD8$^+$ T cells for 72 hours; ****p < 0.0001, Unpaired *t*-test for n = 3 biological replicates. Pooled data are represented as mean ± SEM.

Data information: See also Figure EV1

Figure 2: HOIP-deficient melanoma cells exhibit increased sensitivity to combined TNF and IFN-γ

(A) Representative flow cytometry plots (left) and pooled data (right) of competition assays with sgControl and sg*Rnf31* B16-F10 ova tumor cells after culture with the indicated recombinant

Commented [HG1]: Please define the nature, i.e. biological or technical, of the replicates. Please define the bars and error bars, e.g. mean ± SD.

cytokine(s) (10 ng/mL) for 48 hours; n.s.: no significance, ****p < 0.0001, Unpaired *t*-test for n = 3 biological replicates. Pooled data are represented as mean ± SEM.

(B) CRISPR/Cas9 screen showing depleted B16-F10 genes after one week culture with TNF + IFN-γ (both 10 ng/mL); blue genes indicate overall genes with p < 0.001, black genes indicate genes of interest with p < 0.05. Significance assessed using MAGeCK test.

(C) Individual $\log_2$-transformed sgRNA count values from (B) for *Rnf31* (left) and *Rbck1* (right); significance assessed using MAGeCK test.

(D) GO term analysis showing enriched biological processes for the top depleted genes from (B).

(E) TNF/IFN-γ and NK cell CRISPR/Cas9 screen comparison showing shared depleted genes; indicated genes are p < 0.01 and filtered for 3/4 affected sgRNA in both screens.

(F) TNF/IFN-γ and OT-I CRISPR/Cas9 screen comparison showing shared depleted genes; indicated genes are p < 0.001 and filtered for 3/4 affected sgRNA in both screens.

(G) Western blot analysis on whole cell lysates showing HOIP expression for sgControl and sg*RNF31* A375 tumor cells created using CRISPR/Cas9; β-actin was used as a loading control.

(H) Representative flow cytometry plots (left) and pooled data (right) showing PI staining of sgControl or sg*RNF31* A375 tumor cells after culture with the indicated recombinant cytokine(s) (10 ng/mL) for 48 hours; n.s.: no significance, *p < 0.05, **p < 0.01, Unpaired *t*-test for n = 3 biological replicates. Pooled data are represented as mean ± SEM.

Commented [HG2]: Please define the nature, i.e. biological or technical, of the replicates. Please define the bars and error bars, e.g. mean ± SD.

Data information: See also Figure EV2 and Dataset EV1

Figure 3: Combined TNF and IFN-γ induces transcription-dependent apoptosis in HOIP-deficient cells that requires both intrinsic and extrinsic apoptotic machinery

(A) PI staining of sgControl or sg*Rnf31* B16-F10 tumor cells treated with combined TNF/IFN-γ (both 10 ng/mL) for 24 hours in the absence and presence of QVD-OPh (10 μM); n.s.: no significance, ***p < 0.001, ****p < 0.0001, Unpaired *t*-test for n = 3 biological replicates. Pooled data are represented as mean ± SEM.

(B) Western blot analysis of the indicated proteins on whole cell lysates for sgControl or sg*Rnf31* B16-F10 tumor cells cultured with the indicated cytokine(s) (10 ng/mL for all) for 0, 3, 6, or 9 hours; β-actin was used as a loading control.

(C) Schematic outlining experimental design of CRISPR/Cas9 screening for sg*Rnf31* B16-F10 resistance to killing by combined TNF/IFN-γ (both 10 ng/ml).

(D) CRISPR/Cas9 screen showing enriched genes from sg*Rnf31* B16-F10 tumor cells after successive treatment with combined TNF/IFN-γ, as described in (C); red genes indicate overall genes with $p < 0.0001$. Significance assessed using MAGeCK test.

(E) Individual log_2-transformed sgRNA count values from (D) for genes associated with classical IFN-γ (top) and TNF (bottom) signaling; significance assessed using MAGeCK test.

(F) GO term analysis showing enriched biological processes for the top enriched genes from (D); the top 10 terms are displayed.

(G) PI staining of sgControl, sg*Rnf31*, sg*Rnf31*/*Stat1*, sg*Rnf31*/*Casp8*, sg*Rnf31*/*Bid*, or sg*Rnf31*/*Rela* B16-F10 tumor cells treated with combined TNF/IFN-γ for 24 hours; $*p < 0.05$, $****p < 0.0001$, asterisk(s) indicated group vs TNF/IFN-γ-treated sg*Rnf31* group, Unpaired *t*-test for $n \geq 3$ biological replicates. Pooled data are represented as mean ± SEM.

Data information: See also Figure EV3 and Dataset EV2

Figure 4: Pharmacological inhibition of HOIP sensitizes tumor cells to combined TNF and IFN-γ induced apoptosis *in vitro*

(A) Representative flow cytometry plots (left) and pooled data (right) showing PI staining of parental B16-F10 tumor cells left untreated or treated with recombinant TNF/IFN-γ (both 10 ng/mL) for 48 hours, following a 4 hour pre-treatment with vehicle or HOIPIN-1 (50 μM) (the concentration of vehicle/HOIPIN-1 was halved upon the addition of cytokines); n.s.: no significance, $**p < 0.01$, Unpaired *t*-test for n = 3 biological replicates. Pooled data are represented as mean ± SEM.

(B) Representative flow cytometry plots (left) and pooled data (right) showing PI staining of parental B16-F10 tumor cells left untreated or treated with supernatant (Sup) (derived from a previous overnight OT-I/B16-F10 ova co-culture at the indicated E:T ratio for 48 hours, following a 4 hour pre-treatment with vehicle or HOIPIN-1 (50 μM) (the concentration of vehicle/HOIPIN-1 was halved upon the addition of Sup); $*p < 0.05$, $**p < 0.01$, Unpaired *t*-test for n = 3 biological replicates. Pooled data are represented as mean ± SEM.

(C) Representative flow cytometry plots (left) and pooled data (right) showing PI staining of parental A375 tumor cells left untreated or treated with TNF/IFN-γ (both 10 ng/mL) for 48 hours, following a 4 hour pre-treatment with vehicle or HOIPIN-1 (50 μM) (the concentration of vehicle/HOIPIN-1 was halved upon the addition of cytokines); $*p < 0.05$, $**p < 0.01$, $****p < 0.0001$, Unpaired *t*-test for n = 3 biological replicates. Pooled data are represented as mean ± SEM.

Data information: See also Figure EV4

Commented [HG3]: Please define the nature, i.e. biological or technical, of the replicates. Please define the bars and error bars, e.g. mean ± SD.

Commented [HG4]: Please define the nature, i.e. biological or technical, of the replicates. Please define the bars and error bars, e.g. mean ± SD.

Figure 5: HOIP-deficient tumors exhibit enhanced OT-I-mediated control *in vivo*

(A) Experimental design of *in vivo* model with subcutaneous B16-F10 ova tumors treated with adoptive OT-I therapy.

(B) Individual (left) and average (right) *in vivo* growth of subcutaneous wild-type or sg*Rnf31* B16-F10 ova tumors left untreated or treated with adoptively transferred OT-I $CD8^+$ T cells (on days indicated by black arrows); *p < 0.05, **p < 0.01, Unpaired *t*-test for OT-I-treated wild-type vs OT-I-treated sg*Rnf31* with n = 5/6 mice per group. Pooled data are represented as mean ± SEM.

(C) Overall survival of mice from (B); *p < 0.05, **p < 0.01, Log-rank test.

Data information: See also Figure EV5

EXPANDED VIEW LEGENDS

Commented [HG5]: Please define the error bars, e.g. SEM

Figure EV1: Additional validation of HOIP-deficient tumor cells

(A) Representative flow cytometry histograms (left) and pooled data (right) of H-2K^b expression on sgControl or sg*Rnf31* B16-F10 ova tumor cells before and after overnight exposure to IFN-γ (5 ng/mL); *p < 0.05, Unpaired *t*-test for n = 3 biological replicates. Pooled data are represented as mean ± SEM.

(B) *In vitro* proliferation of sgControl or sg*Rnf31* B16-F10 ova tumor cells over 4 days; n = 3 biological replicates. Pooled data are represented as mean ± SEM.

Figure EV2: Additional validation of TNF and IFN-γ in mediating cell death of HOIP-deficient tumor cells

(A) 24 hour IFN-γ (left) and TNF (right) secretion in supernatant by NK cells from competition assays performed with sgControl/sg*Rnf31* B16-F10 ova tumor cells; n.s.: no significance, Unpaired *t*-test for n = 3 biological replicates. Pooled data are represented as mean ± SEM.

(B) 24 hour IFN-γ (left) and TNF (right) secretion in supernatant by OT-I cells from competition assays performed with sgControl/sg*Rnf31* B16-F10 ova tumor cells; **p < 0.01, ****p < 0.0001, Unpaired *t*-test for n = 3 biological replicates. Pooled data are represented as mean ± SEM.

(C) Outline (top) of experimental setup for cytokine pre-treatment competition assays and pooled data (bottom) showing proportion of sgControl or sg*Rnf31* B16-F10 ova tumor cells after pre- and post-treatments as outlined; all cytokines were used at 10 ng/mL; **p < 0,01; Unpaired *t*-test for n = 3 biological replicates. Pooled data are represented as mean ± SEM.

(D) Representative flow cytometry histograms (left) and pooled data (right) of competition assays with sgControl and sg*Rnf31* B16-F10 ova tumor cells after culture with supernatant (Sup), derived from a previous overnight OT-I/B16-F10 ova co-culture (0.25 E:T ratio), for 24 hours in the absence and presence of neutralizing α-TNF and α-IFN-γ antibodies (both 10 µg/mL); n = 2 biological replicates

(E) *In vitro* proliferation of sgControl or sg*RNF31* A375 tumor cells over 4 days; n.s.: no significance, Unpaired *t*-test for n = 3 biological replicates. Pooled data are represented as mean ± SEM.

Figure EV3: Additional validation of proteins involved in apoptosis of HOIP-deficient tumor cells induced by combined TNF and IFN-γ

(A) PI staining of sgControl or sg*Rnf31* B16-F10 tumor cells after treatment with the indicated cytokine(s) (10 ng/mL) for 24 hours; n.s.: no significance, **p < 0.01, ****p < 0.0001, Unpaired *t*-test for n = 3 biological replicates. Pooled data are represented as mean ± SEM.

Commented [HG6]: Please define the nature, i.e. biological or technical, of the replicates. Please define the error bars, e.g. SD.

Commented [HG7]: Please define the nature, i.e. biological or technical, of the replicates. Please define the bars and error bars, e.g. mean ± SD.

Commented [HG8]: Please define the nature, i.e. biological or technical, of the replicates.

Commented [HG9]: Please define the nature, i.e. biological or technical, of the replicates. Please define the bars and error bars, e.g. mean ± SD.

(B) Individual sgRNA count values from sg*Rnf31* B16-F10 resistance screen performed with combined IFN-γ + TNF for genes associated with DISC assembly. Significance assessed using MAGeCK test.

(C) Western blot analysis of whole cell lysates showing expression of Bax and Bak in the indicated B16-F10 cell line; β-actin was used as a loading control.

(D) PI staining of sgControl, sg*Rnf31*, or sg*Rnf31/Bax/Bak1* B16-F10 tumor cells after treatment with IFN-γ + TNF (both 10 ng/mL) for 24 hours; n.s.: no significance, **p < 0.01, ***p < 0.001, Unpaired *t*-test for n = 3 biological replicates. Pooled data are represented as mean ± SEM.

(E) Western blot analysis on whole cell lysates showing expression of STAT1, caspase-8, Bid, and p65 (left to right), in the indicated B16-F10 cell line created using CRISPR/Cas9; β-actin was used as a loading control.

(F) PI staining of sgControl or sg*Rnf31* B16-F10 tumor cells treated with combined TNF/IFN-γ (both 10 ng/mL) for 24 hours in the absence and presence of 1400W (20 μM); n.s.: no significance, **p < 0.01, ***p < 0.001, Unpaired *t*-test for n = 3 biological replicates. Pooled data are represented as mean ± SEM.

Figure EV4: Additional HOIPIN-1 experiments and relevance of *RNF31* in other tumor types

(A) IFN-γ (left) and TNF (right) secretion by OT-I cells after 24 hour co-culture with B16-F10 ova tumor cells, following a 4 hour pre-treatment with vehicle or HOIPIN-1 (50 μM) (the concentration of vehicle/HOIPIN-1 was halved upon the addition of IFN-γ + TNF); n.s.: no significance, Unpaired *t*-test for n = 3 biological replicates. Pooled data are represented as mean ± SEM.

(B) Representative flow cytometry plots (left) and pooled data (right) showing PI staining of HeLa tumor cells left untreated or treated with recombinant IFN-γ + TNF (both 10 ng/mL) for 48 hours, following a 4 hour pre-treatment with vehicle or HOIPIN-1 (50 μM) (the concentration of vehicle/HOIPIN-1 was halved upon the addition of cytokines); n.s.: no significance, *p < 0.05, Unpaired *t*-test for n = 3 biological replicates. Pooled data are represented as mean ± SEM.

(C) *RNF31* expression in TCGA tumor types assessed using TIMER v1; gray columns indicate cancer types were normal tissue or metastasis data are available; n.s.: no significance, *p < 0.05, **p < 0.01, ***p < 0.001, Wilcoxon test for n ≥ 9 biological replicates per group. Central band of boxplot represents median, box represents the interquartile range (IQR), and whiskers represent upper and lower limits relative to the IQR. Specific numbers of data points per group are displayed along the x-axis.

Figure EV5: Additional *in vivo* tumor growth data

Commented [HG10]: Please define the nature, i.e. biological or technical, of the replicates. Please define the bars and error bars, e.g. mean ± SD.

Commented [HG11]: Please define the nature, i.e. biological or technical, of the replicates. Please define the bars and error bars, e.g. mean ± SD.

Commented [HG12]: Please define the central band, boxes and whiskers of the boxplot. Please define the number and the nature, i.e. biological or technical, of the replicates.

Additional experiment showing individual (left) and average (right) *in vivo* growth of subcutaneous wild-type or sg*Rnf31* B16-F10 ova tumors treated with adoptively transferred OT-I CD8 T cells (on days indicated by black arrows); *p < 0.05, Unpaired *t*-test with n = 5/6 mice per group. Pooled data are represented as mean ± SEM.

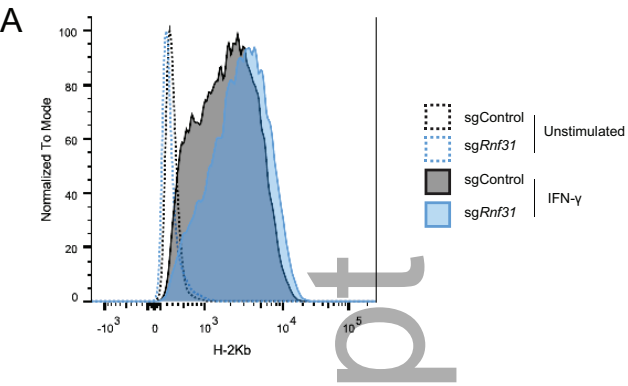

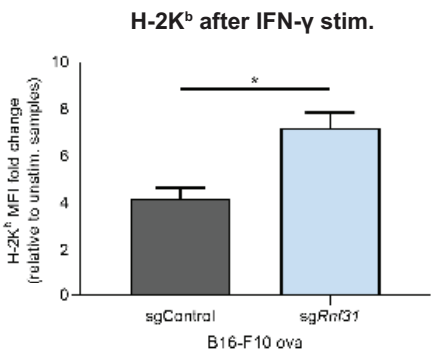

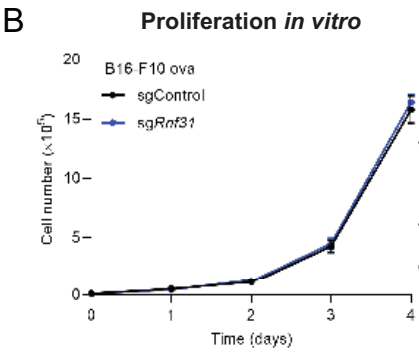

embr_202153391_f1ev.eps

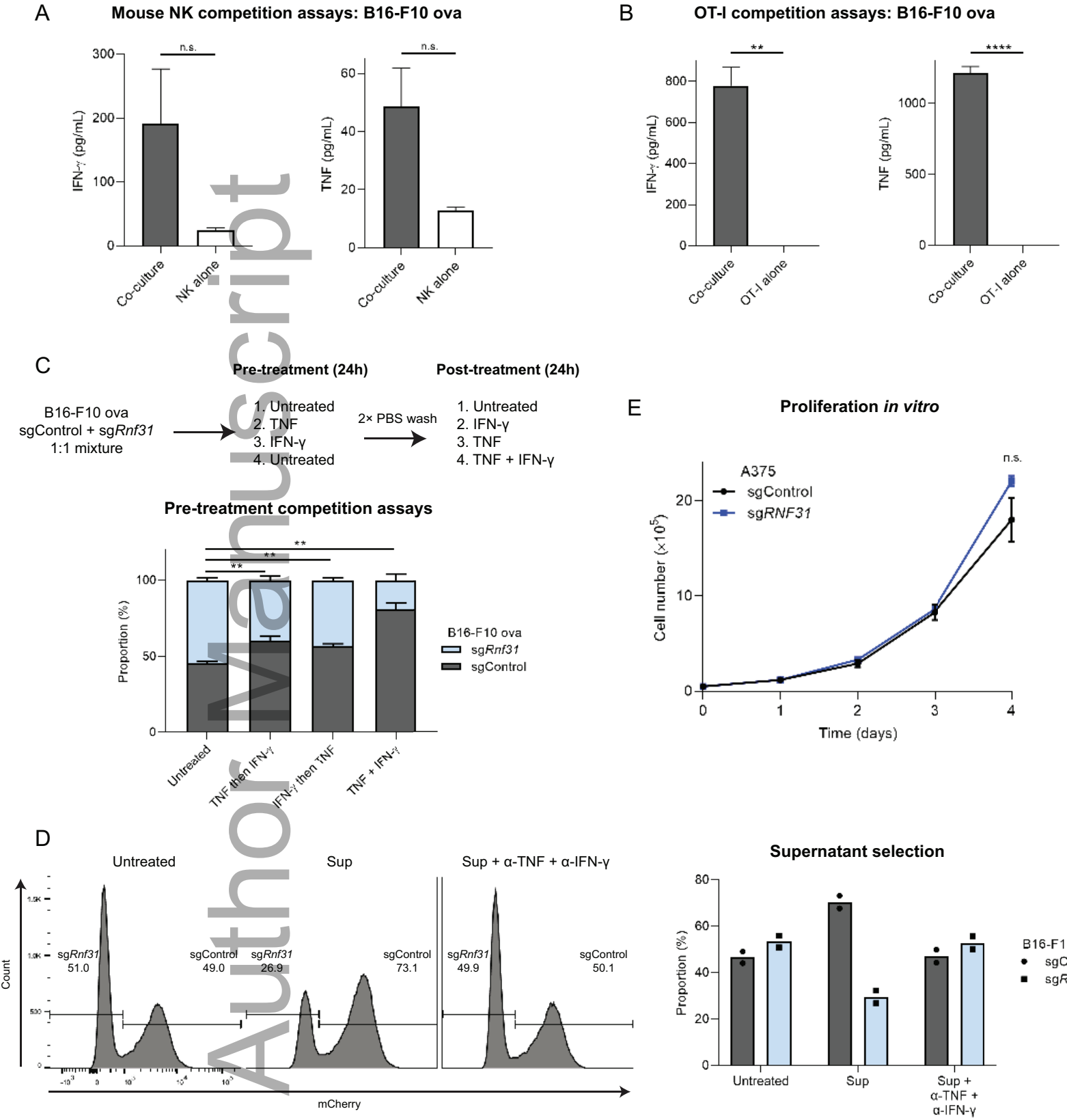

embr_202153391_f2ev.eps

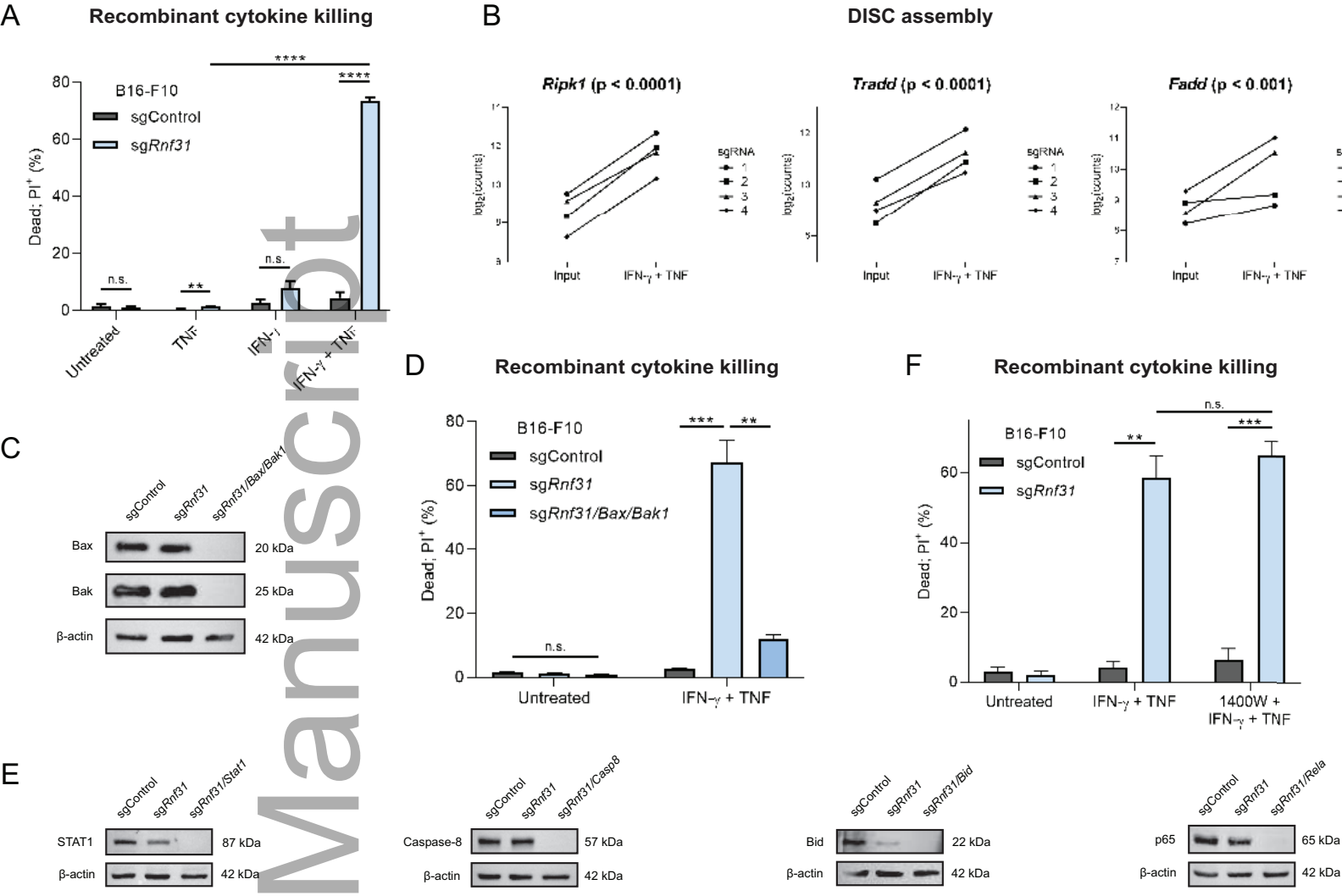

embr_202153391_f3ev.eps

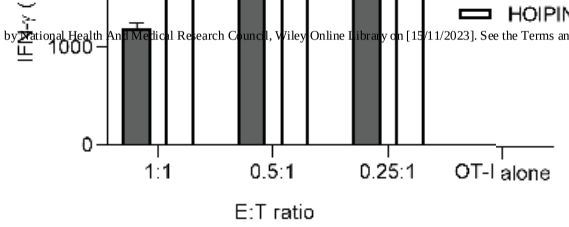

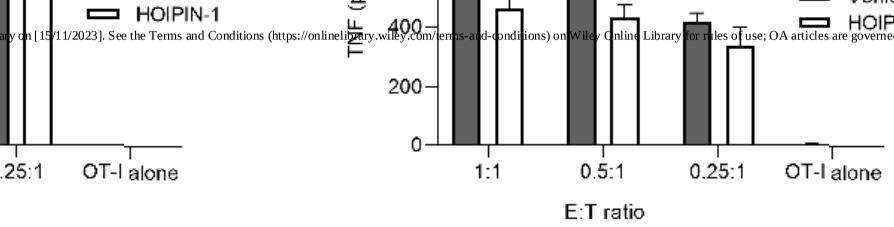

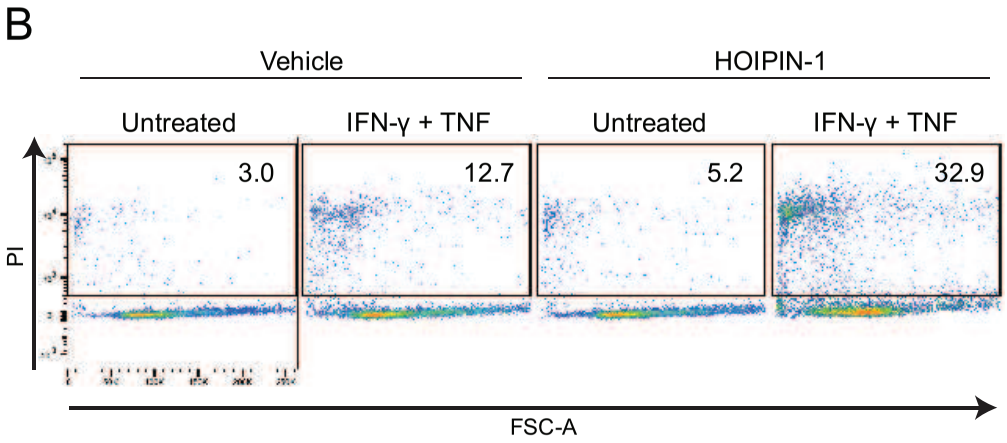

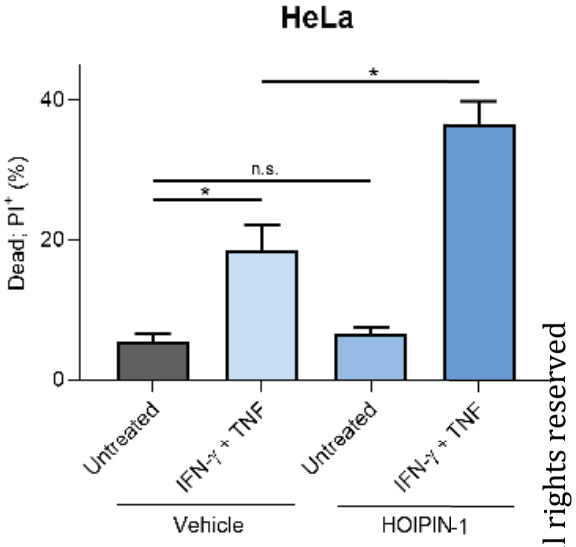

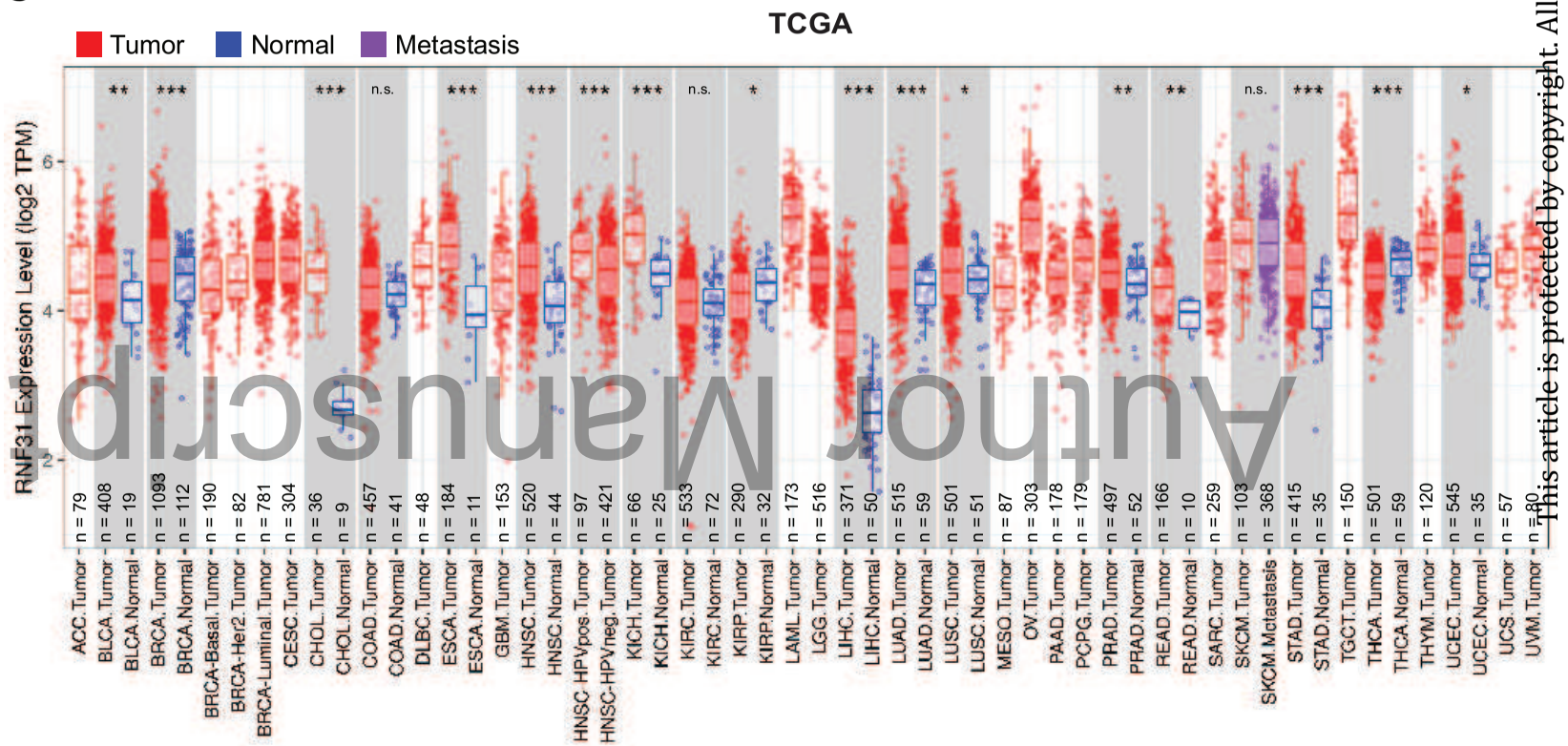

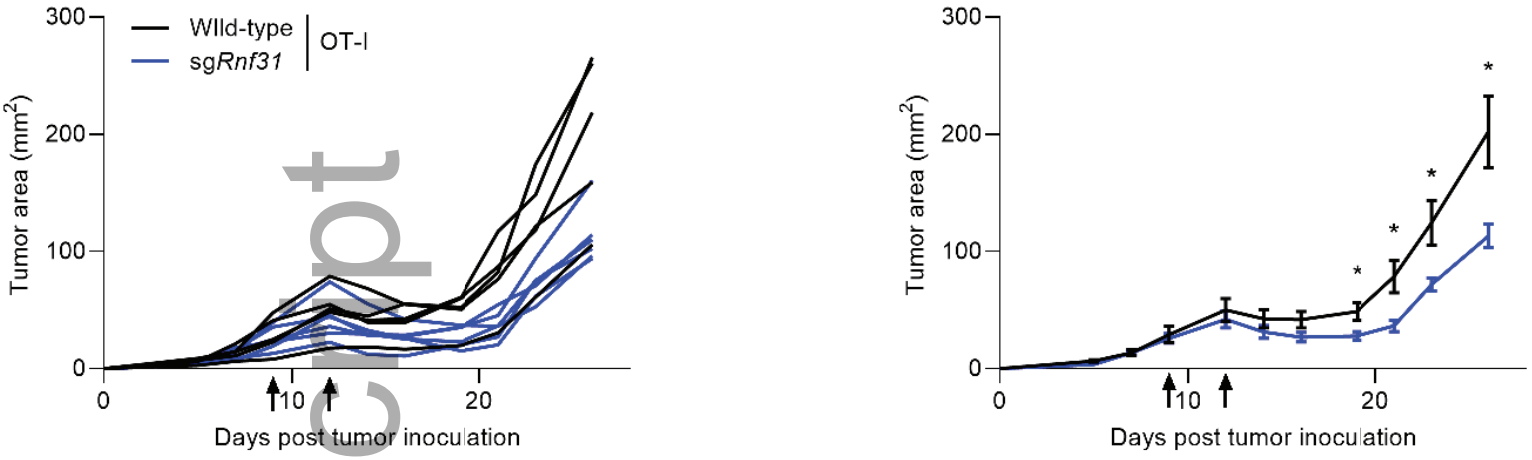

embr_202153391_f5ev.eps

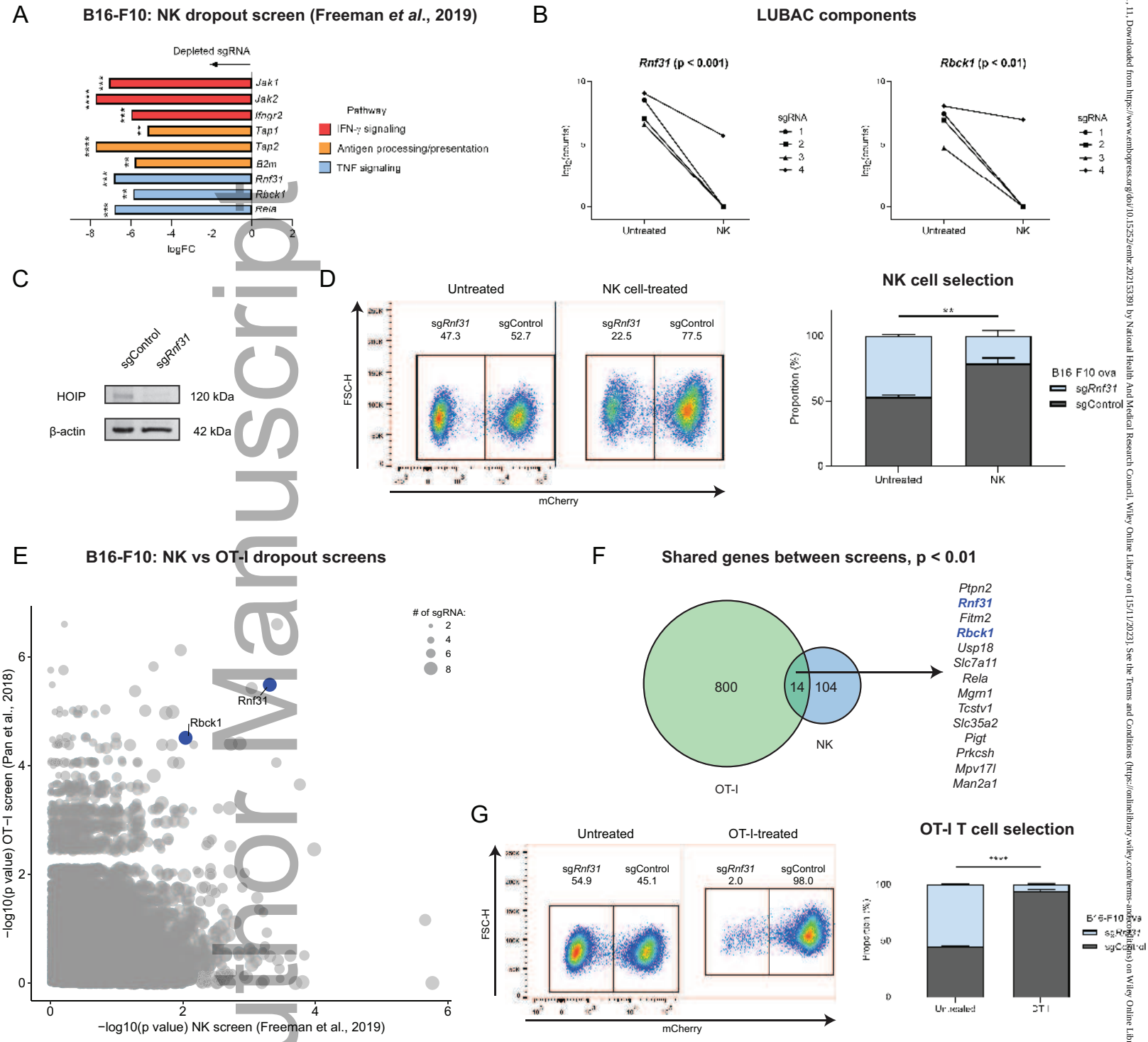

embr_202153391_f1.eps

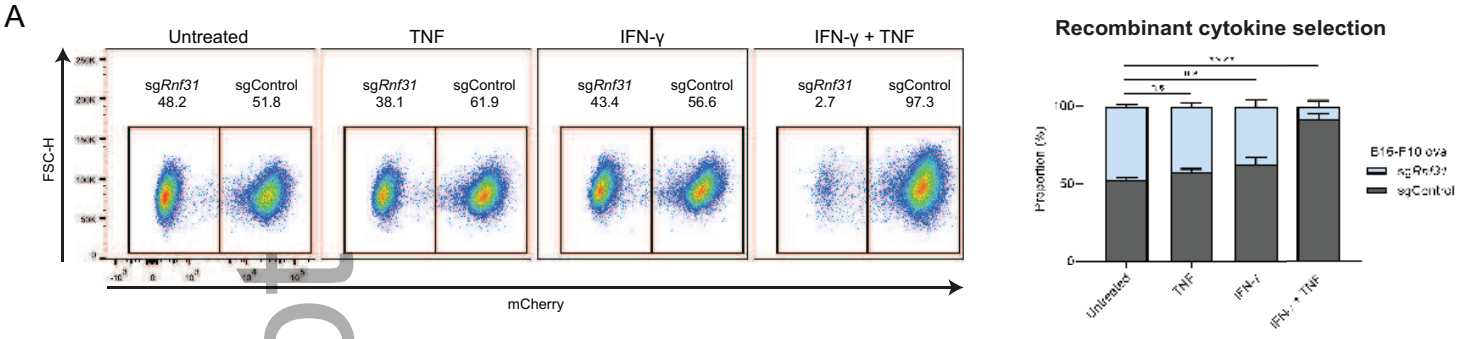

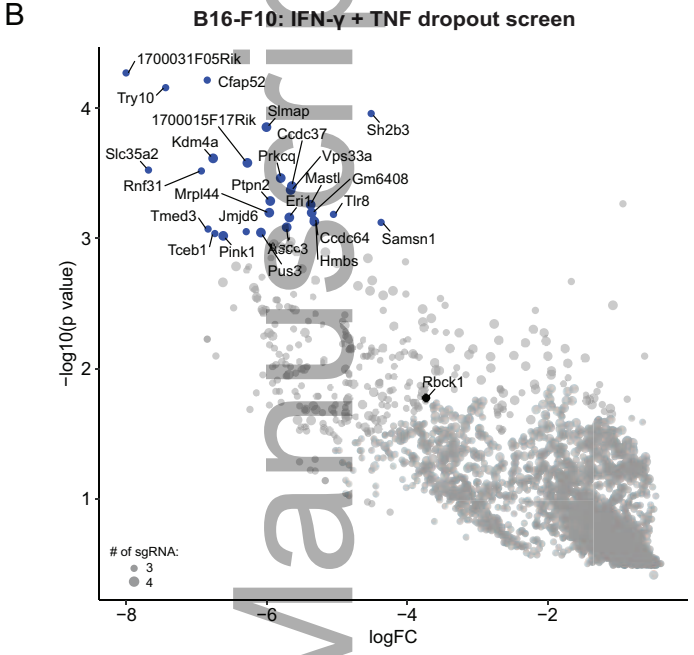

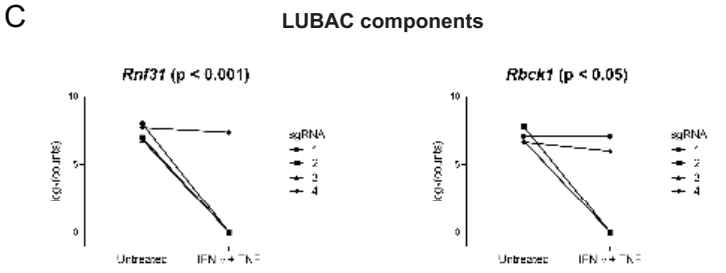

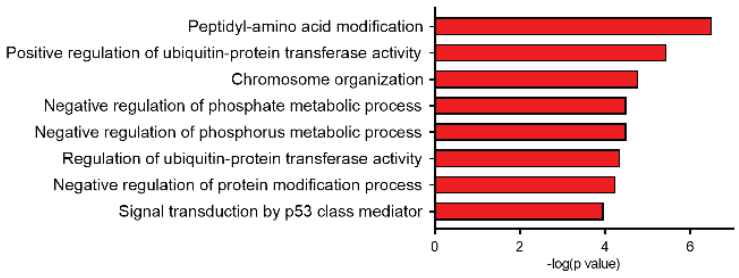

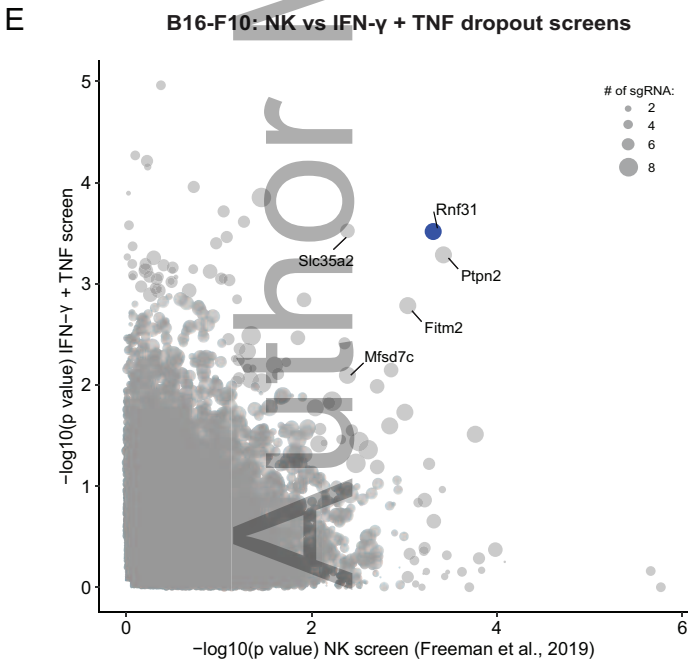

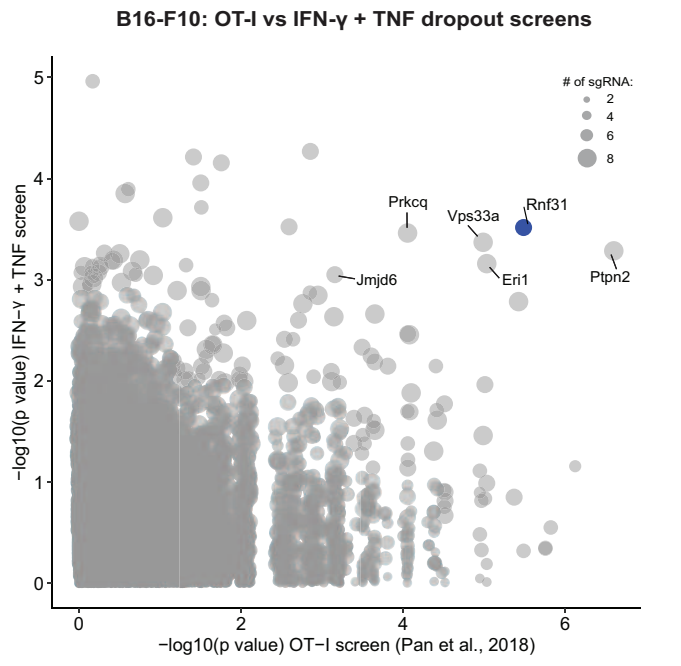

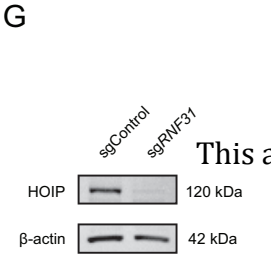

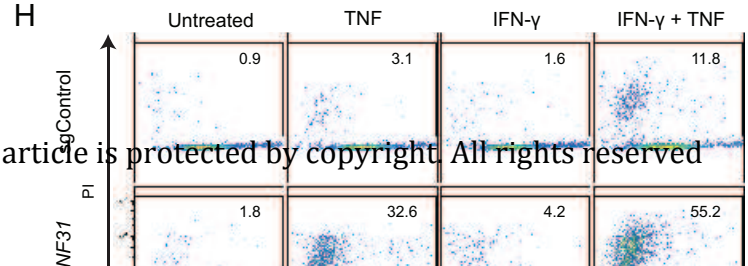

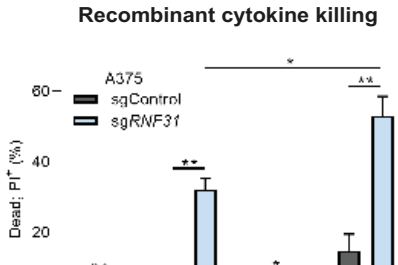

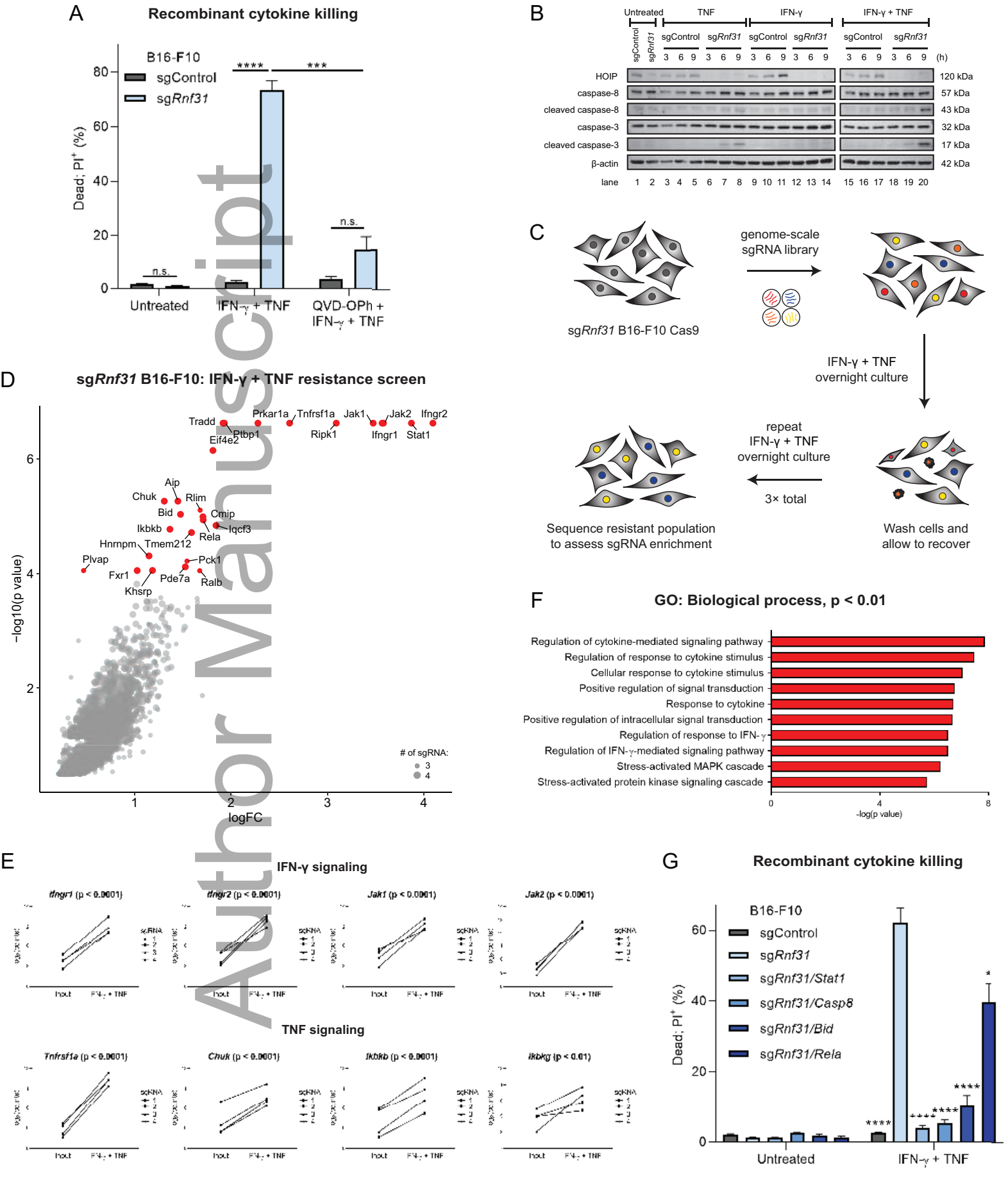

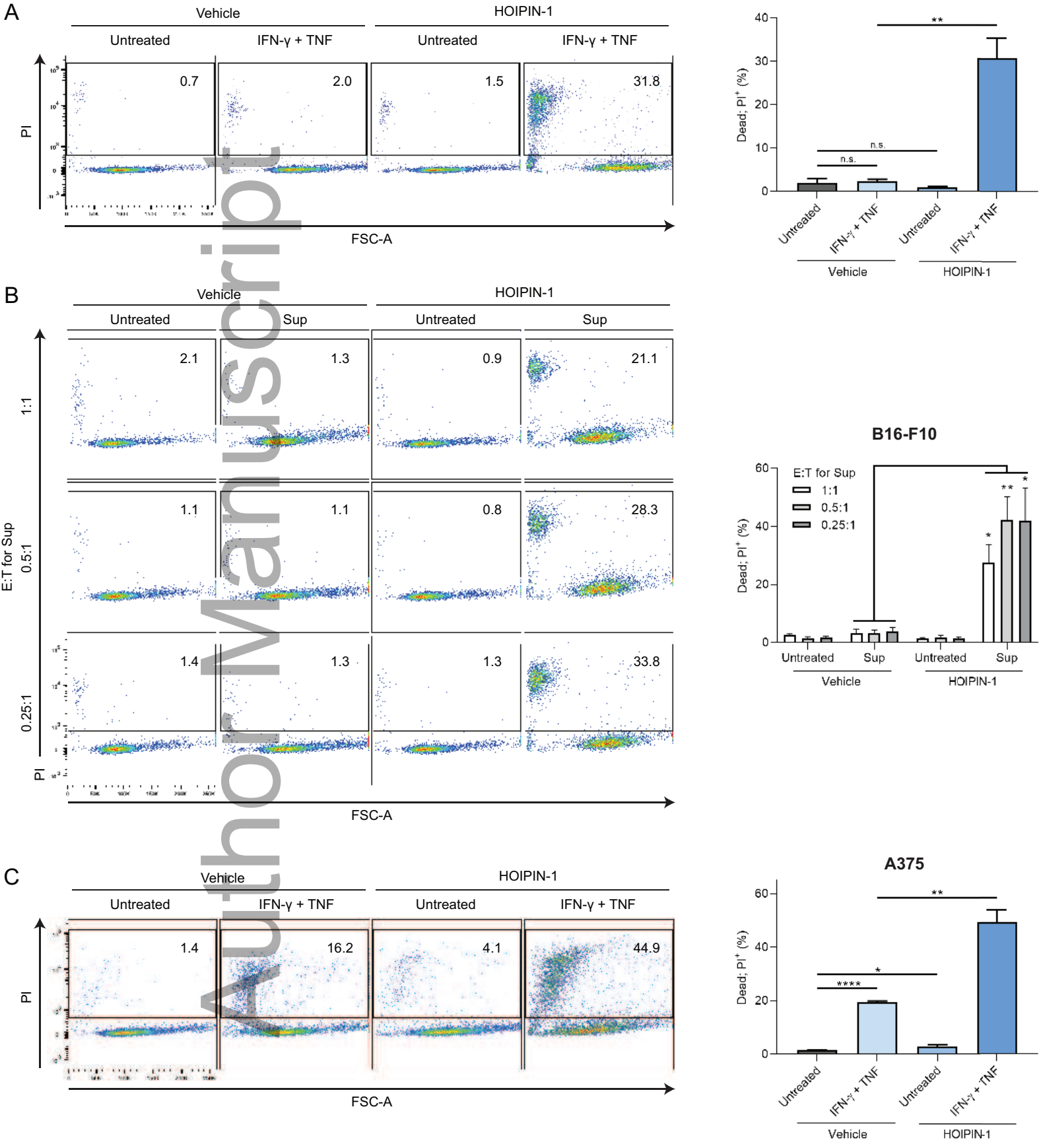

embr_202153391_f4.eps

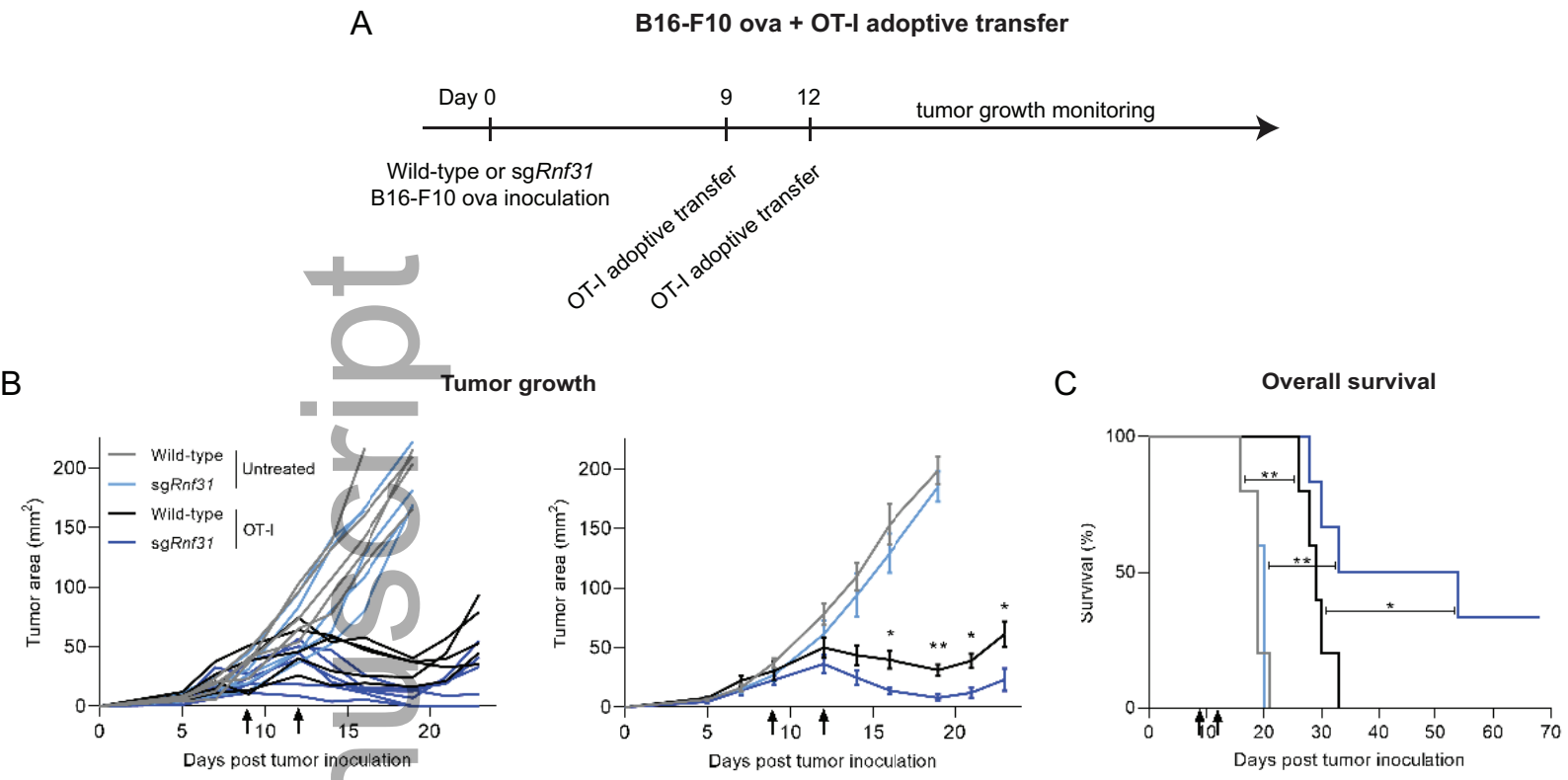

embr_202153391_f5.eps